New insights from fully-integrated surface-subsurface hydrological modeling in high-elevation glaciated environments

Xinyang Fan[1,2], Florentin Hofmeister[3,4], Bettina Schaefli[1], and Gabriele Chiogna[2]

[1]Institute of Geography and Oeschger Centre for Climate Change Research, University of Bern, Bern, Switzerland
[2]Department of Geography and Geosciences, GeoZentrum Nordbayern, Friedrich-Alexander-University Erlangen-Nuremberg, Erlangen, Germany
[3]Chair of Hydrology and River Basin Management, School of Engineering and Design, Technical University of Munich, Munich, Germany
[4]Bavarian Academy of Sciences and Humanities, Munich, Germany

Correspondence: Xinyang Fan (xinyang.fan@unibe.ch)

Abstract. Recent modeling efforts go towards distributed physics-based modeling for improved hydrological process understanding. The sparse hydro-meteorological observations and complex topography in high-elevation mountainous environments have, however, hampered the application of such data-intensive and sophisticated techniques for detailed process exploration. In particular, characterizing surface-subsurface water exchange processes in these terrains remains understudied. Here we implement a fully-integrated and fully-distributed surface-subsurface hydrological model, *WaSiM*, to quantify the observed daily streamflow variations and their interactions with groundwater in the high-elevation glaciated catchment (Martell Valley) in the central European Alps since the 2000s. Extensive field observations (meteorology, vegetation, glacier mass balance, soil properties, river discharge), especially in-situ groundwater levels, were collected to investigate hydrological processes and constrain model parameters in the surface and subsurface. We observe that in contrast to the delayed responses typically observed in aquifers, shallow alpine groundwater responds nearly as quickly as streamflow to peak snowmelt and extreme rainfall events, highlighting the need for improved subsurface parametrization in hydrological modeling. Surprisingly, model simulations with limited subsurface lateral flow (interflow, in the unsaturated zone) contribution best fit the observed groundwater levels and streamflow, suggesting that groundwater flow, in combination with surface runoff, is dynamic enough to explain the observed daily streamflow dynamics in the computational settings. Moreover, to overcome the challenges of integrating point-scale groundwater observations into a fully-distributed hydrological model in high-elevation catchments, we suggest pre-calculating the Topographic Wetness Index to guide piezometer placement. Despite the inherent uncertainties associated with the necessary assumptions of modeling, this study sheds new light on surface-subsurface hydrological processes in high Alpine landscapes.

1 Introduction

With rising temperatures and increasing frequency and intensity of hydrological extremes, many regions worldwide are experiencing severe impacts of climate change (IPCC, 2021). Mountain glaciers are among the most sensitive indicators of climate change, with widespread glacier retreat and declining snowfall observed globally (Rounce et al., 2023; Matiu et al., 2021;

Marcolini et al., 2017). These changes threaten downstream water availability, hydropower production, and ecosystem functioning, while increasing risks associated with glacier-related hazards such as glacial lake outburst floods (Drenkhan et al., 2023; Wechsler et al., 2023; Schaefli et al., 2019; Banerjee et al., 2024). Therefore, improving our understanding of hydrological processes and water storage changes in high-elevation environments is essential for projecting future water resource availability and associated societal impacts (van Tiel et al., 2024).

Hydrological models have been widely used to assess climate change impacts on alpine water resources. Many applications rely on lumped-parameter or semi-distributed models, such as HBV, mHM, and THREW-T (Seibert and Bergström, 2022; Nan et al., 2021; Kumar et al., 2013). These models have successfully reproduced catchment-scale runoff responses but generally represent subsurface processes using simplified conceptual approaches, such as one-dimensional linear reservoirs or direct drainage from soil layers to streams without a groundwater module (Coderre et al., 2026; Horton et al., 2022; Fatichi et al., 2015; Dobler and Pappenberger, 2013; Schaefli et al., 2005; Coderre et al., 2026). Consequently, groundwater storage, recharge, and baseflow generation are often poorly represented, introducing uncertainties in projections of future hydrological change (Puspitarini et al., 2020; Tuo et al., 2018). In particular, streamflow simulations in high-alpine catchments frequently show deficiencies in representing winter baseflow and the timing of melt-driven runoff increases (Michel et al., 2022; Schaefli et al., 2014; Schaefli and Huss, 2011).

Improving streamflow simulations in mountain environments has traditionally focused on improving snow representation, as errors in snow distribution and melt timing are commonly considered major sources of uncertainty (Freudiger et al., 2017; Warscher et al., 2013; Dobler and Pappenberger, 2013). However, recent evaluations suggest that many snow models can reproduce observed snow dynamics reasonably well (Hofmeister et al., 2022; Carletti et al., 2022; Schlögl et al., 2016). This indicates that deficiencies in alpine hydrological simulations may also originate from missing processes or oversimplified model structures, particularly the representation of groundwater and surface–subsurface interactions (Somers and McKenzie, 2020). Despite the recognized importance of groundwater in regulating streamflow variability, its role in high-alpine hydrological systems remains poorly constrained because groundwater observations are scarce and subsurface properties are highly uncertain (van Tiel et al., 2024; Müller et al., 2024; Fan et al., 2023a; Hofmeister et al., 2023a).

Quantifying groundwater–surface water interactions remains challenging in mountainous regions due to complex topography, geology, and coupled surface–subsurface processes, with additional complexities introduced by snow and glacier melt in cryosphere-dominated environments (Abhervé et al., 2023; Fan et al., 2023b; Krause et al., 2007). Accordingly, the widely accepted runoff-generation classification by Dunne (1983) indicates that, in humid climates and steep terrain, runoff generation is commonly dominated by lateral subsurface stormflow in combination with saturation-excess overland flow (Trancoso et al., 2016). However, the streamflow generation process in the steep terrain in the cryosphere is still not fully understood and whether the Dunne diagram is applicable in such environment (Trancoso et al., 2016; Dunne, 1983). Recent studies have investigated groundwater storage, geological controls on groundwater dynamics, and physically based representations of surface–subsurface interactions in alpine catchments (Müller et al., 2024; Engdahl, 2024; Chen et al., 2023; Thornton et al., 2022; Arnoux et al., 2021; Somers et al., 2016). However, the challenges remain: semi-distributed models lack sufficient spatial resolution to capture heterogeneous groundwater responses (Chen et al., 2023), whereas fully distributed approaches require detailed hydrogeolog-

ical information and substantial computational resources that are often unavailable in high-alpine environments (Thornton et al., 2022; Engdahl, 2024). Consequently, only a limited number of studies have applied integrated surface–subsurface hydrological models in cryosphere-dominated alpine catchments. Thornton et al. (2022) coupled *WaSiM* (Schulla, 2024, 1997) with *HydroGeoSphere* (Aquanty, 2016) to investigate groundwater–cryosphere interactions and highlighted the importance of near-surface processes in regulating meltwater and rainfall partitioning between surface and subsurface pathways. More recently. Aubry-Wake et al. (2024) applied a fully-integrated hydrological response unit (HRU)-based framework - *Cold Regions Hydrological Modelling Platform* (Pomeroy et al., 2007) to investigate cryosphere-surface water–groundwater interactions but did not quantify the overland flow and subsurface lateral flow ("interflow", in the unsaturated zone) contributions to streamflow separately, while van Tiel et al. (2024) emphasized the broader challenges of representing groundwater processes in glaciated environments. Despite these advances, fully-distributed and fully-integrated modeling applications remain rare due to limited hydrogeological observations and the challenges associated with model implementation, parameterization, and calibration.

Fully-integrated hydrological models provide an opportunity to explicitly represent interactions among ice, snow, soil moisture, surface water, and groundwater processes. However, their application in high Alpine environments remains challenging because the model states and fluxes are spatially distributed, whereas observations are generally available only at discrete locations (Fatichi et al., 2016). Nevertheless, in-situ observations remain essential for model calibration and evaluation. Snow depth observations help constrain snow accumulation and melt in distributed hydrological models (Ruelland, 2024; Thornton et al., 2021); in-situ soil moisture measurements provide information on vadose-zone storage dynamics (Vereecken et al., 2008); and groundwater level observations offer unique insight into subsurface storage and interactions between groundwater and surface water (Bonotto et al., 2022). However, groundwater observations are often the most limited in high-elevation glaciated environments, making them one of the least available but most valuable data sources for evaluating integrated hydrological models (Borzi, 2025). Therefore, developing and evaluating integrated models using available groundwater observations is critical for improving process understanding in glaciated catchments.

To address these crucial knowledge gaps, this study presents one of the first applications of a fully-distributed and fully-integrated surface–subsurface hydrological modeling approach in a high-elevation glaciated catchment. The *WaSiM* model (Schulla, 2024, 1997) is adopted as it is one of the very few fully-distributed and fully-integrated hydrological models suitable for modeling the high-elevation glaciated environments. By explicitly representing unsaturated-zone and groundwater flow processes and constraining the model with extensive hydro-meteorological observations, including rare in-situ groundwater level measurements, we investigate surface–subsurface hydrological processes and storage dynamics in the Martell Valley (Northern Italy). Beyond evaluating model performance, this study aims to assess what new insights can be obtained from an integrated modeling framework regarding water partitioning between the surface and subsurface domains, while also identifying the limitations and practical challenges associated with applying such models in data-scarce mountain regions.

Specifically, this study addresses the following questions: (i) Can a fully-distributed and fully-integrated hydrological model reproduce both streamflow and groundwater dynamics in a high-elevation glaciated catchment? (ii) What new insights into surface–subsurface water exchange and hydrological processes can be obtained from such a detailed modeling framework?

(iii) What are the opportunities and limitations of applying fully-distributed and fully-integrated hydrological models under the observational data constraints typical of high Alpine environments?

2 Study site

The Martell Valley is a high-elevation glaciated catchment in the central European Alps (Northern Italy, see Fig. 1a,b) with an elevation range of 1777 to 3743 m a.s.l (mean: 2737 m a.s.l.) and complex fine-scale topography. The catchment has an area of 77 km^2 including 9 subcatchments (S1-S9) and it is closed at the Zufritt Lake. It is covered by around 34% of grassland (growing upon shallow soil formation), 9% of forests, 17% of glaciers, and 40% area of exposed rocks and soil (CORINE Land Cover, 2018) (Fig. 1c). The glaciers are mainly located in the southwest of the catchment, with the largest being Langenferner, Zufallferner, and Fürkeleferner. These glaciers reached their largest extension during the last Little Ice Age (LIA). Glacier retreat has been observed since the 1850s and accelerated since the 1980s (Knoflach et al., 2021). It is one of the key drivers of high-alpine geosystem changes, such as land cover, ecological succession, hydrology, and geomorphology (Ramskogler et al., 2023; Knoflach et al., 2021).

We derived the catchment hydrogeology information based on the dominant geological characteristics available in the geology map and geodatabase (Fig. 1a) (Ramskogler et al., 2023; Berra et al., 2012). In the mapping area (except Subcatchment S1 due to lack of data), the rock units take 35% (likely presence of fractured and fissured aquifers) and the sedimentary units take 45% (likely presence of porous aquifers); the rest of the information under the glacier is unavailable. The dominant rock units are orthogneiss, phyllite, quartz, and marble (Ramskogler et al., 2023; Berra et al., 2012). Climatically, this catchment is relatively dry among the European Alps (Höge et al., 2023; Ceperley et al., 2020; Isotta et al., 2018). It has a mean annual temperature of -1.2°C between 2007 and 2023, with the maximum of 0.2°C in 2022 and the minimum of -2.9°C in 2010 (based on the interpolated catchment mean, Section 3.1). The mean annual precipitation and modeled evapotranspiration (Section 3.1) are 1048 mm yr^{-1} and 167 mm yr^{-1} for the same period. 2014 is the wettest year, with the highest annual precipitation of 1368 mm and the lowest evapotranspiration of 122 mm. 2022 is the driest year, with the lowest annual precipitation of 661 mm and the highest annual evapotranspiration of 218 mm.

Most of the hydro(geo)logical stations are located in the upper Subcatchments S7–S9, which comprise a proglacial outwash plain in the form of an alluvial fan (Fig. 1). As the majority of the stations are situated in this area, our primary study focus is on these subcatchments, with the model calibrated to the observations from this region. However, the modeling results are presented both for the upper subcatchments in detail (with higher confidence) and for the entire catchment to provide an overview (with lower confidence). This decision is motivated by the fact that prior studies in Martell Valley are interested in the streamflow in both upper subcatchments and at the catchment outlet (Schaffhauser et al., 2024; Brighenti et al., 2023).

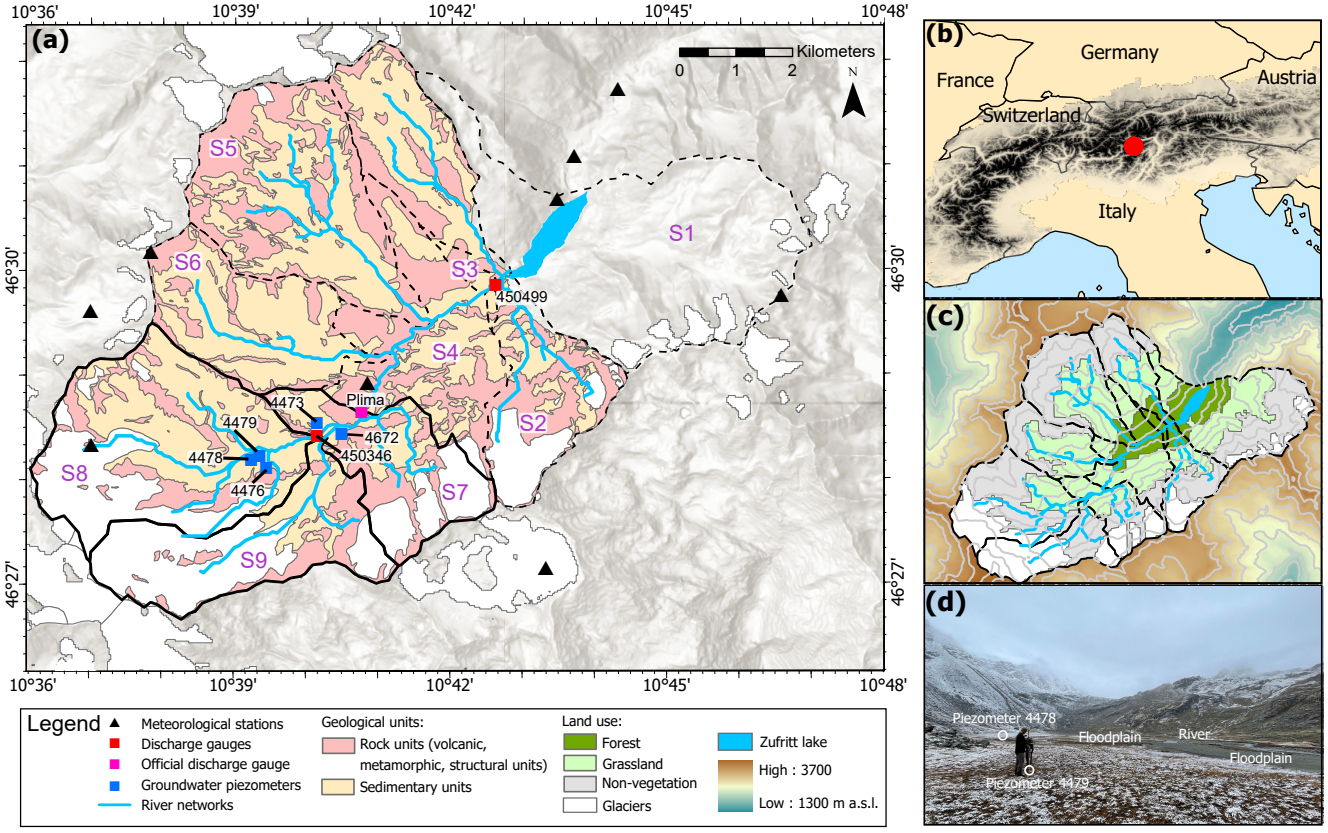

Figure 1. Maps of the Martell Valley in Northern Italy: (a) The zoomed-in map with the observed hydro-meteorological stations, with background characterized by geological units (Ramskogler et al., 2023; Berra et al., 2012). The numbers in black refer to the hydrological station IDs listed in Table 2 and the numbers (S1-S9) in violet refer to the subcatchment IDs. The white blocks denote the regional glacier coverage in 2000 (Knoflach et al., 2021). (b) The overview map shows the location of Martell Valley in the central European Alps. The dark shadow denotes the European Alps (Jarvis et al., 2008) and the red dot denotes the catchment location. (c) The land use map of the catchment (CORINE Land Cover, 2018): forest, grassland, glaciers (in 2006), and area exposed with rocks and soil (non-vegetation), with background characterized by Digital Elevation Model data and contour lines (di Bolzano Alto Adige, 2006). (d) Fieldwork photo taken in November 2023 in the Subcatchment S8 (>2400 m a.s.l.) where the piezometers ID 4478 and 4479 are located.

3 Observed temporal and spatial data

3.1 Meteorological data

The daily meteorological station data are measured and used as inputs in the *WaSiM* hydrological model. 12 stations (Tab.1 and Fig.1a) are located in and around the Martell Valley with records of air temperature, precipitation, solar radiation, relative humidity, wind speed, and snow height from 1972 to 2024. The elevations of all stations vary from 1720 to 3328 m a.s.l.

Hofmeister et al. (2023a) assessed the data quality and corrected the observation errors of these climate stations until 2020. We apply the same procedure to the extended time series between 2020 and 2024.

The spatial and temporal interpolation of the climate station data to the retained spatial grid (25m × 25m) is performed in the *WaSiM* modeling environment. *WaSiM* supports irregularly observed data (i.e., missing values) and uses the following interpolation methods: the solar radiation, relative humidity, and precipitation recorded at the observed stations are spatially interpolated at daily time steps with the Inverse Distance Weighting (IDW) method. The wind speed and air temperature are interpolated with a combined method of IDW and elevation-dependent regression. The potential evapotranspiration (PET) is calculated with the Penman-Monteith method (Brutsaert, 1982; Monteith, 1981) available in *WaSiM* by using the daily temperature, relative humidity, solar radiation, and wind speed.

The snow height (SH) data are measured at the Zufritt and Zufallhuette stations (Tab. 1). We transform the snow height to snow water equivalent (SWE) with the ΔSnow model (v1.0.2) available in the R package "*nixmass*" (Winkler et al., 2021). This model adopts a process-based multi-layer method and considers the relationship between snow density (Pistocchi, 2016) and predefined regional parameters for Italy (Guyennon et al., 2019) in the SWE calculation. The SWE data are then used to calibrate the parameters of the snow module in *WaSiM* (Details on snow module calibration are given in Section 4.1).

Table 1. Meteorological stations with daily records near the Martell Valley. Abbreviations: mean air temperature (T in [°C]), precipitation (P in [mm]), solar radiation (GS in W m^{-2}), relative humidity (LF in %), wind speed (WS in [m s^{-1}]), snow height (SH in [cm]).

Station name	Station ID	Longitude [°]	Latitude [°]	Elevation [m a.s.l.]	Start date	End date	Climate variables
Schoentaufspitze	06040WS	10.6286	46.5029	3328	2003.01.01	2024.01.15	T, WS
Madritsch	06090SF	10.6144	46.4938	2825	2003.01.01	2024.01.15	T, P, GS, LF, WS
Sulden	06400MS	10.5953	46.5159	1907	2003.01.01	2024.01.15	T, P, GS, LF
Hintermartell	11400MS	10.7269	46.5169	1720	2009.01.01	2024.01.15	T, P, GS, LF, WS
Weissbrunnspitz	24170WS	10.7740	46.4940	3253	2004.01.01	2024.01.15	T, P, GS, LF, WS
Rossbaenke	24300SF	10.8194	46.4693	2255	2002.01.01	2024.01.15	T, LF, WS
Weissbrunn	24400MS	10.8318	46.4868	1900	2002.01.01	2024.01.15	T, LF
Careser	T0065	10.6991	46.4226	2600	1990.10.01	2024.01.15	T, P, LF, WS
Ghiacciaio	T0473	10.7183	46.4513	3093	1990.12.01	2024.01.15	T, LF, WS
Langenferner	-	10.6139	46.4725	2967	2012.10.26	2023.10.02	T, GS, LF, WS
Zufritt	11200BM	10.7251	46.5090	1851	1972.01.01	2024.01.15	T, P, SH
Zufallhuette	16ZH	10.6781	46.4814	2265	2004.12.01	2023.02.23	SH

3.2 Hydro(geo)logical data

We installed five groundwater piezometers in the river floodplains, which are relatively flat with the pre-assumed existence of groundwater storage (Fig. 1 and Tab. 2). The piezometers are located at elevations above 2300 m a.s.l. and in the same

geological units (alluvial and fluvioglacial deposits, alpine postglacial synthemes, quaternary aquifer) (Ramskogler et al., 2023; Berra et al., 2012). We also installed two river gauging stations which cover an elevation range of 1878 to 2347 m a.s.l. (Fig. 1 and Tab. 2). The river water levels are transformed to discharge with the rating curves of Hofmeister et al. (2023b). The main river (Plima) has its source at the Langenferner, flows through the catchment, and enters the Zufritt Lake in the northeast. The Plima official discharge station has been operated since 2014. All groundwater level and river discharge data are preprocessed in daily time steps for the hydrological model simulations.

Additionally, we collected groundwater and river water samples at the Piezometers ID 4478, 4479, and Stream gauge ID 450346 in the upper Subcatchment S8 in November 2022 and November 2023 to understand surface water-groundwater interactions at the onset of the low-flow season. The stable water isotopes (δ^2H and δ^{18}O) are analyzed in the laboratory in the Institute of Geography at the University of Bern with the cavity ringdown spectrometer "Picarro L2140-i" with autosampler and the attached vaporisation module "Picarro A0211". We follow the procedure described in the work of Meier (2024) (Sect.3.2.1) to perform laboratory analysis of water samples and preprocessing of the isotope data.

We quantify the trends of the time-series hydrological variables with the non-parametric Mann-Kendall test (Kendall, 1955; Mann, 1945) and Sen's slope method (Sen, 1968). Statistical significance is assessed at the 5% level (p-value < 0.05) and uncertainty in the slope estimates is characterized using 95% confidence intervals (CI). The MATLAB function *mannkendall* (v1.0.0) (Collaud Coen and Vogt, 2021; Collaud Coen et al., 2020) is adopted to first remove the first-order autocorrelation in the data with a 3PW pre-whitening procedure and then to quantify the trends.

Table 2. Observed groundwater piezometers and river gauging stations in the Martell Valley. The Plima Station is an official station operated by the Autonomous Province of Bolzano in South Tyrol. The river gauge ID 450499 was destroyed during the extreme flooding events between 12 July and 9 August 2023.

Variable	Station ID	Longitude [°]	Latitude [°]	Elevation [m a.s.l]	Start date	End date
Groundwater	4478	10.65186	46.46949	2454	2022.11.24	2023.11.01
Groundwater	4479	10.65302	46.47014	2455	2022.11.24	2023.11.01
Groundwater	4476	10.65507	46.46828	2447	2023.05.12	2023.11.01
Groundwater	4473	10.66646	46.47441	2333	2023.03.29	2023.11.01
Groundwater	4672	10.67205	46.47382	2319	2023.09.20	2023.11.01
River	450346	10.66730	46.47256	2347	2019.07.17	2023.11.01
River	450499	10.70838	46.49637	1878	2020.06.30	2023.08.07
River	Plima	10.67680	46.47630	2311	2014.06.01	2024.01.15

3.3 Spatial data

The Digital Elevation Model (DEM) data of the study site are provided by the Province of Bolzano (di Bolzano Alto Adige, 2006) and available in a spatial resolution of 0.5 m × 0.5 m in 2006. The soil profile and attributes in 2018 are extracted from the Harmonized World Soil Database (HWSD, version 2.0) in a 1 km × 1 km resolution (FAO & IIASA, 2023; Ramskogler et al.,

2023). The land use and land cover data of the site in 2018 are obtained from the Corine Land Cover Data Center (CORINE Land Cover, 2018) in a resolution of 100 m $\times$ 100 m (Fig.1c). The geology map and geodatabase of the site are obtained from Ramskogler et al. (2023) and Berra et al. (2012). The glacier coverage maps of the site are obtained from Knoflach et al. (2021) and are available in the years 1850, 1911, 1959, 1985, 1997, 2005, 2013, 2017, and 2019.

All spatial raster data are resampled to the same spatial resolution with *ArcGIS Pro* (v3.1.0) for hydrological modeling. We adopt the modeling spatial resolution of 25m $\times$ 25m (after testing with 20m, 50m, 100m) by balancing the trade-off between the computational intensity and the terrain complexity. As for many comparable high-elevation catchments, there is no detailed soil data available at this site. The available soil data may struggle to represent some small-scale features (e.g., moraine or similar glacier deposits) due to limited resolution (FAO & IIASA, 2023; Ramskogler et al., 2023).

We use the add-on software of *WaSiM* named *Tanalys* to generate the spatial grid data of local slope and flow accumulation based on the DEM data. These two variables are then used to calculate the Topographic Wetness Index (TWI) for each grid cell in the catchment to facilitate understanding the topographic control of the hydrological processes by using Eq. 1 (Pourali et al., 2016; Beven and Kirkby, 1979):

$$\text{TWI} := \ln\left(\frac{a}{\tan\beta}\right), \tag{1}$$

where a [m^2] is the local upslope catchment area per unit contour length along the flow pathway; $\tan\beta$ is the local steepest downslope in radians by comparing the slope of the modeled grid cell with that of its neighboring cells.

4 Fully-integrated surface-subsurface hydrological modeling

We run the Water Balance Simulation Model (*WaSiM*) (Schulla, 2024, 1997) version 10.08.00 in daily time step and 25 m $\times$ 25 m spatial resolution. Different versions of the model have previously been used in many studies, such as for investigating fast local infiltration (Bronstert et al., 2023), snow process and redistribution (Förster et al., 2018; Warscher et al., 2013), impact of land use changes on streamflow (Cornelissen et al., 2013), and flash floods in the Mediterranean catchments (Garambois et al., 2013), but to our knowledge it has not been fully applied yet in high-elevation environments. *WaSiM* is a 2-dimensional, fully-distributed, and modular-based hydrological model. It simulates hydrological partitioning and fluxes on a regular horizontal grid, with the stream network being represented as selected grid cells of the domain. The subsurface consists of a predefined number of soil layers, with groundwater situated at the bottom. Groundwater heads can fluctuate between these layers (Schulla, 2024). Lateral exchange is allowed between the soil grid cells that are adjacent to the stream network cells. The Darcy's law is implemented to simulate groundwater flow in the groundwater module (Schulla, 2024).

Besides the meteorological time series (air temperature, precipitation, solar radiation, wind speed, relative humidity), *WaSiM* also requires spatial gridded inputs, such as local slope, aspect, flow direction, flow accumulation, and river networks. These raster files are generated with *Tanalys* (Schulla, 2024) based on the DEM data. Each module in *WaSiM* can be flexibly activated depending on research needs. A detailed description of each module is available in the works of Schulla (2024, 1997). Here, we

focus on describing the key modules used to set up the fully-integrated surface-subsurface hydrological model in the Martell Valley, including the snow, glacier, unsaturated zone, and groundwater modules.

4.1 Snow and glacier modules

In *WaSiM* version 10.08.00 (Schulla, 2024), the snowfall is simulated with a threshold approach and a user-defined temperature-transition range. For snowmelt, we adopt the advanced energy-balance method together with the wind-driven and gravitational snow redistribution algorithms (Schulla, 2024; Thornton et al., 2021; Shrestha et al., 2014; Warscher et al., 2013; Gruber, 2007). This enables improved snow and river discharge simulations (Fig. S1 in the Supplementary Materials) compared with the commonly adopted temperature-index approach (Fan et al., 2026; Liu et al., 2025; Nan et al., 2025). The disadvantage of this approach is the significantly increased computational demand and simulation time. The outflow from the snowpack infiltrates into the soil, which is solved with the Richards equation (Richards, 1931). The infiltration amount is the minimum between the fillable porosity of the uppermost soil layer and the total amount of rainfall and meltwater per time step. Surface runoff is generated by the infiltration excess and saturation excess of the soil moisture.

We adopt the dynamic glacier module (Schulla, 2024) to simulate the glacier area evolution by using a volume-area scaling approach (Bahr et al., 1997; Chen and Ohmura, 1990). In the glacier module, the glacier mass gain (due to snow accumulation) and melt (due to snow, firn, and ice melt) are calculated and balanced over each year in *WaSiM*. The transformation from snow to firn takes one year if the snow does not melt within one season, and from snow to ice takes seven years (Schulla, 2024). The model calculates the annual glacier mass balance, updates the glacier cover, and simulates snow metamorphism on 1 October of each year. The snow-on-ice melt is simulated with the same energy-balance approach as adopted in the Snow Module. As the energy-balance method is not available for simulating ice melt in *WaSiM*, we adopt the extended temperature-index approach (Hock, 1999, 1998) which allows us to include the solar radiation information at each daily time step when simulating the firn and ice melt (see Eqs.2.21.2 and 2.21.3 in the work of Schulla (2024)). The meltwater from snow-on-ice, firn, and ice is conceptually transformed into streamflow via a linear reservoir approach: each melt component is handled with a separate linear reservoir that has a specific storage coefficient (Schulla, 2024). We acknowledge the modeling uncertainty associated with the simplified assumption of the drainage systems in glaciers during each melting period.

4.2 Unsaturated zone and groundwater model

All grid cells that are not stream grid cells contain a fixed number of unsaturated and saturated domain layers, which is set to five in total here (this applies also to glacier grid cells). Input to the unsaturated zone module is the sum of non-intercepted rainfall and meltwater from snow and ice (if present). Infiltration and vertical fluxes between the unsaturated soil layers are solved iteratively with the Richards equations (Schulla, 2024, 1997; Richards, 1931). The properties for each soil layer and for each soil type (i.e. soil in alpine grassland, podzol under coniferous forest, rocks) are defined per grid cell, such as soil depth, vertical hydraulic conductivity, and characteristics of the macropores (e.g., macropore capacity, reduction of macropore capacity per meter of soil depth) (Schulla, 2024). The macropore approach is implemented in *WaSiM* by following the "bypass-flow-concept" introduced in the work of Jansson and Karlberg (2011).

To simulate the groundwater head changes, the unsaturated zone is coupled with a horizontal 2-dimensional groundwater model. Groundwater is situated at the bottom of the soil layers. For this reason, *WaSiM* requires the lower boundary of the aquifer to be identical to the lower boundary of the soil layers. The shallow aquifer is modelled as unconfined, given that the observed depth to water table (DTW) is mostly within 1 m. The unsaturated zone module first computes the vertical flux (i.e., the percolation) from the lowest unsaturated soil layer to the groundwater. This flux is then taken as the upper boundary condition for the groundwater model to calculate the lateral fluxes, which are solved with the Darcy equation. The net changes of the groundwater table are converted into a vertical flux, which is given back to the lowest unsaturated soil layer as inflow or outflow (Schulla, 2024). Five parameters in the groundwater model are calibrated with the observed groundwater heads measured at the piezometers (Tab.4), including the horizontal hydraulic conductivities, storage coefficient, lower boundary of the aquifer, and colmation of the soil, which is a term used in *WaSiM*: it controls the water exchange rate between the adjacent saturated soil cells and the stream network cells. The groundwater heads are assumed to be constant beneath the glacierized cells, which is a built-in feature in the model (Schulla, 2024).

4.3 Streamflow generation

The generation of streamflow based on water mobilized at the level of grid cells follows two stages: First, the surface runoff and the subsurface lateral flow ("interflow", in the unsaturated zone) are computed per grid cell; they are then transformed separately to the stream by a single reservoir cascade (isochrone approach with additional retention in each class, see details in Schulla (2024)). *WaSiM* applies a flow travel time concept at each time step in the reservoir cascade to ensure temporal synchronization of each flow component (Eq.2.12.13 in the work of Schulla (2024)). The surface runoff is generated when saturation excess of soil moisture or Hortonian infiltration excess occurs. The subsurface lateral flow for each layer per grid cell is generated based on the water content of the soil layer, hydraulic conductivity, and local slope. Baseflow contribution to streamflow is obtained via direct lateral exchange of adjacent saturated soil cells to stream cells. The stream grid cells are generated with the add-on *Tanalys* software of *WaSiM* based on the DEM data; they correspond to the actual observed stream locations as closely as possible. The average values of each streamflow component (surface runoff, subsurface lateral flow, and baseflow) are summed up to the total streamflow, which is the input to the routing model (Schulla, 2024).

4.4 Model calibration and evaluation

4.4.1 Calibration parameters

Here we summarize the parameters to be calibrated in each module of *WaSiM*. In the snow module, 11 key parameters that govern snow accumulation, snow ablation, wind-driven and gravitational snow redistribution are calibrated (Tab.3). Specifically, the calibrated parameters "TRS" and "Ttrans" (0°C and 2°C) define a linear transition of snow fraction from 100% at -2°C ("Ttrans"), 50% at 0°C ("TRS"), to 0% at +2°C ("Ttrans"). In the glacier module, 7 key parameters that govern the initialization of glacier volume and the ice and firn melt are calibrated (Tab.3). The average equilibrium line elevation (ELA, m a.s.l.) in the model is set to 2900 m a.s.l. based on the observations at the Langenferner glacier in 2006 (Autonome Province

of Bolzano, 2007). The volume-area scaling factor is set to 28.5, adopted from the work of Chen and Ohmura (1990), and the exponent is set to 1.375 according to the work of Bahr et al. (2015).

The parameters in the subsurface module are calibrated using the observed groundwater heads at the piezometers in the upper headwater subcatchments (S7-S9, Fig.1). The lower boundary of the soil layers is calibrated to be 1.30 m (see details in Sect.S3 and Fig. S4-S8 in the Supplementary Materials); the properties for each soil layer (vertical heterogeneity) and each soil type (i.e. soil in alpine grassland, podzol under coniferous forest, rocks, for representing horizontal heterogeneity) are defined per grid cell, such as hydraulic conductivity and characteristics of the macropores. In the groundwater model, the aquifer hydraulic conductivity, storage coefficient, and colmation of the soil are calibrated. A total of 13 parameters are calibrated and their values are provided in Table 4. Many calibrated groundwater parameters are found to be identical at the 5 piezometers, likely due to similar local geology and water fluctuation depths (Fig. 1 and Sect.2). Initial sensitivity analyses indicate that the remaining parameters are rather insensitive; the default values suggested for each soil type from the user manual (Schulla, 2024) are hence adopted for them. This study focuses on the upper subcatchments (S7-S9), where the majority of hydrological stations and groundwater piezometers are installed and where the simulated results have high confidence. Nevertheless, we also modeled the whole catchment by transferring the subsurface parameters from the upper subcatchments to the ungauged area with the aim of providing a catchment-scale overview, while acknowledging that the overview results may contain higher uncertainty, especially in the valley floor due to a lack of deep groundwater observations.

Table 3. Calibrated parameters in the snow and glacier modules in *WaSiM* (Schulla, 2024, 1997). Parameters with no unit are denoted with [-].

Module	Parameter	Description	Value
Snow accumulation	TRS	Temperaure at which half of the precipitation falls as snow [°C]	0
Snow accumulation	Ttrans	Half of the temperature range from snow to rain [°C]	2
Snow ablation	LWINcorr	Correction factor for incoming long-wave radiation [-]	1.2
Snow ablation	LWOUTcorr	Correction factor for outgoing long-wave radiation [-]	1.0
Snow gravitational redistribution	i_lim	Max. deposition slope [°]	55
Snow gravitational redistribution	D_lim	Scaling for max.deposition [mm]	2
Snow gravitational redistribution	i_erosion	Min. slope for creating slides [°]	50
Snow gravitational redistribution	f_erosion	Fraction of snow pack forming the slide [-]	0.007
Wind-driven redistribution	Start azimuth	First quantile of wind direction [°]	179
Wind-driven redistribution	End azimuth	Third quantile of wind direction [°]	217
Wind-driven redistribution	cmin	Min. correction factor [-]	0.5
Glacier initialisation	VA_scale	Volume-area scaling factor [-]	28.5
Glacier initialisation	VA_exp	Volume-area exponential factor [-]	1.375
Glacier initialisation	WEchnge	Change rate of water equivalent per m [mm]	1.8
Glacier initialisation	ELA	Average equilibrium line elevation [m a.s.l.]	2900
Glacier melt	MF	Melt factor [mm]	2
Glacier melt	ice_min	Min. radiation coefficient for ice [mm Wh^{-1} m^2 $°C^{-1}$ day^{-1}]	0.0001
Glacier melt	ice_max	Max. radiation coefficient for ice [mm Wh^{-1} m^2 $°C^{-1}$ day^{-1}]	0.0007

Table 4. Calibrated parameters in the unsaturated zone and groundwater model in *WaSiM* (Schulla, 2024, 1997). Parameters with no unit are denoted with [-]. The hydraulic conductivity (ksat) is calibrated for each land cover category, and the range indicates the variations of hydraulic conductivity between the soil layers vertically. Other parameters are assumed to remain constant, given that all boreholes are situated in the same hydrogeology category.

Module	Parameter	Description	Value
Unsaturated zone	kd	Storage coefficient of direct flow [-]	2
Unsaturated zone	ki	Storage coefficient of subsurface lateral flow [-]	10
Unsaturated zone	dr	Scaling factor applied to river drainage density [-]	0
Soil table	krec	Recession constant for the saturated conductivity with depth [-]	1
Soil table	PMThr	Macropore threshold [mm h^{-1}]	2
Soil table	MRedu	Capacity reduction [m^{-1}]	1
Soil table	Depth	Lower boundary [m]	1.30
Soil table	ksat	Vertical hydraulic conductivity [m s^{-1}]	$4\times10^{-4} \sim 6\times10^{-6}$ (forest area) $2\times10^{-4} \sim 5\times10^{-7}$ (alpine grassland) $1\times10^{-5} \sim 8\times10^{-7}$ (rocks)
Groundwater	Input grid (.aq1)	Lower boundary [m]	1.30
Groundwater	Input grid (.kol)	Colmation of the soil [m s^{-1}]	1×10^{-6}
Groundwater	Input grid (.kx,.ky)	Horizontal conductivity [m s^{-1}]	5×10^{-5}
Groundwater	Input grid (.s03)	Storage coefficient [-]	0.3

4.4.2 Calibration and evaluation procedure

Each model simulation with a selected parameter set runs from 1 October 2006 to 15 January 2024 in a 25 m $\times$ 25 m gridded resolution at daily time steps. Because of long temporal and high spatial resolution adopted for the fully-distributed physics-based modeling, a complete simulation takes around 10 hours to run on a computer with 6 computational cores (Processor: 13th Gen Intel(R) Core(TM) i7-1370P 1.90 GHz). The first 5 years (1 October 2006 - 30 September 2011) are considered as the spin-up period, as the glacier and subsurface water storage modules take time to stabilize to produce reasonable simulations (Hofmeister et al., 2022). The rest (1 October 2011 - 15 January 2024) is used for model calibration and evaluation. Given the large number of parameters, the complicated surface-subsurface hydrological processes (snow-glacier-vegetation-river-unsaturated zone-groundwater), and the complex topography where the elevation ranges around 2000 m (1777 to 3743 m a.s.l.), the computationally intensive automatic calibration is not adopted. Instead, we tackle this task by adopting a multi-signal calibration approach to calibrate the model from top to bottom and module by module with the relevant reference data.

The sequential calibration of module by module is a commonly adopted logical procedure to calibrate fully-distributed physics-based hydrological models (Fatichi et al., 2015). We first analyze the sensitivity of the key parameters in each module. We then perturb and calibrate the identified sensitive parameters in detail to the observed variables.

Specifically, for calibration of the groundwater module using point-scale groundwater level observations, we extracted an ensemble of simulated groundwater level time series from model grid cells located in the vicinity of each observation borehole within the model domain. The resulting ensemble of grid-cell simulations was then compared against the observed groundwater level records at the corresponding borehole locations. Subsurface model parameters were subsequently adjusted based on the discrepancies between simulated and observed groundwater levels to improve model performance.

The module-by-module calibration provides good diagnostic power, as it isolates which modules (e.g., snow, glacier) are causing discrepancies between observation and simulation. This enables an incremental validation, as each module can be tested and validated before being integrated with the next. By doing so, errors in specific processes (e.g., snow or glacier melt) can be addressed without compromising other well-performing modules. Despite the calibration being sequential, we rerun the whole model (including all modules) each time when the parameters in a module are perturbed, and we focus on the model performance of that module. In this way, the hydrological processes between the modules are interconnected and the consistency is ensured. It is worth mentioning that building up a physics-based, fully-distributed hydrological model requires numerous details about the catchment to constrain the model parameters, and it is practically challenging. The purpose of our model is, however, not to reproduce exactly the catchment, but to understand the hydrological processes and to test hypotheses by using a reasonable parameter set, and that the simulated dynamics (relative changes) in the system should be reasonably consistent (Engdahl, 2024).

4.4.3 Reference signals and performance criteria

In the multi-signal calibration, the simulated spatial SWE in *WaSiM* is calibrated to (i) the fractional snow-covered area derived from the MODIS daily snow cover maps (2002-2019) (Matiu et al., 2019) performed by Hofmeister et al. (2022) and (ii) the observed SWE at the in-situ stations from 2006 to 2024 (see Sections 3.1). The glacier module is calibrated to (i) the observed fractional glacier-covered area (which is calculated as the glacier area divided by the catchment area), and (ii) the annual glacier mass balance of the Langenferner glacier (2006-2021) in the Subcatchment S8 (Galos et al., 2017; Autonome Province of Bolzano, 2007). The subsurface modules are calibrated to the observed groundwater hydrographs at the piezometers. The three gauging stations listed in Table 2 are adopted to evaluate the simulated discharge.

We select satisfying model parameters via visual comparison between the simulation and observation for different reference datasets (SWE, discharge, and groundwater heads). We also evaluate the goodness-of-fit of the model with the Nash-Sutcliffe Efficiency (NSE) (Nash and Sutcliffe, 1970), Mean Absolute Error (MAE), and Root Mean Square Error (RMSE). Due to uncertainties in the measured discharge and groundwater heads, the Spearman's rank correlation coefficient (ρ) is also adopted to evaluate the model performance (Gauthier, 2001). Statistical significance is assessed at the 5% level (p-value < 0.05).

5 Results

5.1 Snow and glacier observations and simulations

Figure 2 shows the observed and simulated snow and glacier changes and melt rates in the Martell Valley. The simulated snow water equivalent (SWE) time series extracted from the gridded results capture well the observed snow dynamics at different elevations (Zufritt Station: NSE of 0.87, Spearman's rank correlation coefficient of 0.93 with a p-value < 0.001, MAE of 25.09, RMSE of 50.30. Zufallhuette Station: NSE of 0.74, Spearman's rank correlation coefficient of 0.88 with a p-value < 0.001, MAE of 47.52, RMSE of 60.46). The simulation also reproduces well the interannual variability of snow accumulation and the severe snow droughts in the recent past, for example, with the simulated peak snow accumulation in 2012, 2017, 2022, and 2023 being as low as 138, 103, 112, and 111 mm w.e., which are well below the mean of 316 mm w.e. computed over the evaluation period of 2011-2023 at the Zufritt Station (see Figs. 2a,b). The snow drought in 2022 was observed not only in the Martell Valley but also in the Po Basin in Italy (Avanzi et al., 2024). Hofmeister et al. (2022) adopt the same snow parameter set and show comparable performance between the simulated snow cover and the remote sensing data from Sentinel 2. The simulated snow dynamics and distribution are further used to simulate the hydrological changes in this study.

Like in most glaciated catchments, the observed fractional glacier coverages (glacier area divided by the whole catchment area) are very sparse, but they can still be helpful to understand the glacier module performance (Fig. 2c). The observed fractional glacier coverage shows a declining trend since 1850, except for the period around 1985 showing an increase. The glacier module first takes time to stabilize during the spin-up period (2006-2011). In the evaluation time frame after the spin-up years, the model shows decreasing rates of fractional glacier coverage very close to the observation with a slight overestimation of $\sim$1%. This slightly overestimated glacier coverage is primarily because of a few non-existent small glaciers appearing due to preferential snow deposition along north-east exposed mountain ridges in the model. The simulated catchment cumulative glacier mass balance (zoomed-in plot in Fig. 2c) shows a strong seasonality and a significant decreasing trend of -1.21 m w.e. year^{-1} (p-value < 0.001, 95% CI: -1.39 to -1.10 m w.e. year^{-1} during the evaluation period 2011-2023), which is close to the average glacier mass changing rate (-1.29 $\pm$ 0.28 m w.e. year^{-1} from 2015 to 2024) in central Europe (Dussaillant et al., 2025). Additionally, the glacier module is calibrated to the annual glacier mass balance of Langenferner glacier located in the Subcatchment S8 (Fig.1d). Apart from the spin-up period, the model captures well the general dynamics of the Langenferner glacier mass evolution in both mass-growing years (in 2014) and in loss years. The model simulates well the mean annual glacier mass balance of Langenferner glacier (both simulation & observation are equal to -1.02 m w.e. in the evaluation period between 1 October 2011 and 30 September 2021, Fig. 2d). Nevertheless, it struggles to capture the observations in a few years (i.e., in 2013, 2016, and 2018). This could be because only the Langenferner's glacier mass balance data are available for estimating the parameters of the glacier module. However, glacier mass balance is not only affected by meteorological forcings, but also other environmental factors, such as aspect and elevation (Zhang et al., 2022). Other glaciers in the catchment may hence respond in a slightly different way due to these non-climatic factors (Nan et al., 2025; Müller et al., 2024). Another reason could be that the volume-area scaling factor approach struggles to account for ice flow and tends to underestimate glacier volumetric changes, especially in the accumulation phase (Schaffhauser et al., 2024).

The total annual liquid water input into the catchment (called "precipitation equivalent" or PEQ hereafter) is composed of annual rainfall, snowmelt, and glacier melt. *WaSiM* calculates and outputs the following melt components: snowmelt on the non-glacierized cells, snowmelt on the glacierized cells, firn melt on the glacierized cells, and ice melt on the glacierized cells. The snowmelt reported here is the summed snowmelt occurring both on the glacierized and non-glacierized cells; the reported glacier melt is the summed firn melt and ice melt. Figure 2e shows the annual magnitude of each flux (rainfall, snowmelt, glacier melt) between 2006 and 2023. We quantify the trend of each component starting from 1 October 2011 after the spin-up period. The annual rainfall, snowmelt, and glacier melt amount to 35%, 45%, and 20% of the simulated annual PEQ on average (2011-2023). The PEQ shows a decreasing trend of -21 mm w.e. year^{-1} (p-value = 0.13, 95% CI: -51 to +10 mm w.e. year^{-1}). The estimated annual trends of the flux components are -5 mm year^{-1} for rainfall (p-value = 0.50; 95% CI: -19 to +4 mm year^{-1}), -26 mm year^{-1} for snowmelt (p-value = 0.10; 95% CI: -62 to +4 mm year^{-1}), and +10 mm year^{-1} for glacier melt (p-value = 0.16; 95% CI: -5 to +30 mm year^{-1}). These results indicate that none of the flux components exhibit statistically significant trends over the study period. Among them, snowmelt shows the strongest decreasing tendency, whereas rainfall and glacier melt display comparatively weaker trends. However, the confidence intervals of all three components span both negative and positive values, indicating high uncertainty in the magnitude and direction of the long-term changes.

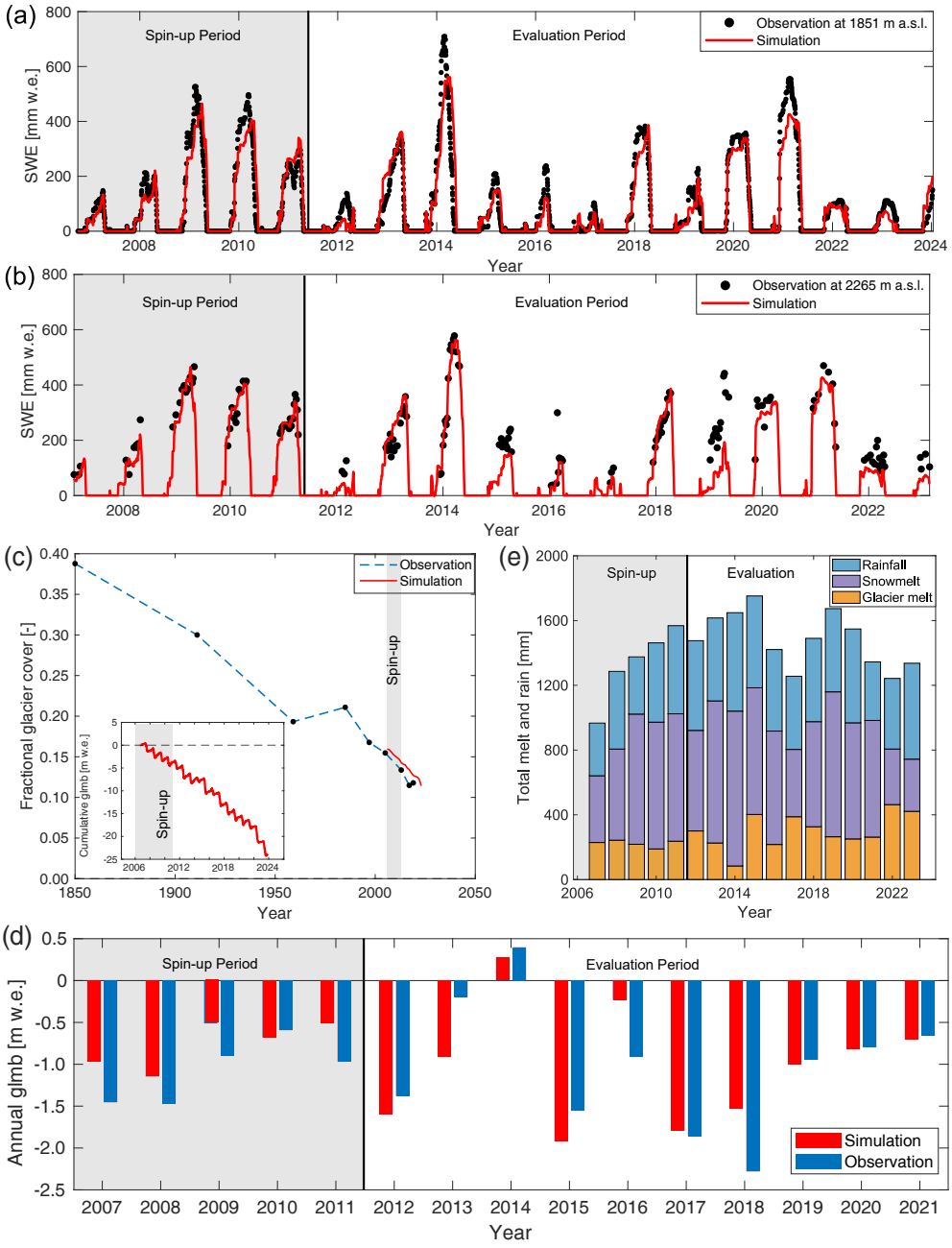

Figure 2. Observed and simulated snow and glacier changes in the Martell Valley. (a-b) The observed and simulated daily snow water equivalent (SWE) in mm w.e. at the (a) Zufritt and (b) Zufallhuette Stations (elevations: 1851 and 2265 m a.s.l. in Table 2). (c) The annual catchment fractional glacier coverage (i.e., glacier area divided by the whole catchment area) observed between 1850 and 2019 and simulated between 2006 and 2023. The zoomed-in plot shows the simulated catchment cumulative glacier mass balance (glmb) between 2006 and 2023. (d) The observed annual glacier mass balance of Langenferner glacier compared with the simulation of Subcatchment S8. (e) The simulated catchment annual total liquid flux (snowmelt, glacier melt, and rainfall) between 2006 and 2023. Spin-up period (5 years): 1 October 2006 - 30 September 2011, evaluation period: starting from 1 October 2011

5.2 Hydro(geo)logical response to peak melts and rainfall events

Figure 3a shows the observed daily river water level and groundwater heads and their responses to the simulated total precipitation equivalent (PEQ) between November 2022 and November 2023 in the upper headwater Subcatchment S8 (subcatchment area: 12.3 km^2 with 31% of glacier coverage, Fig.1a). The groundwater boreholes (IDs 4479 and 4478) have a similar elevation (2455 m and 2454 m a.s.l.) and are both located around 30 m away from the river on the same side (Fig.1 and Tab.2). During the winter between November 2022 and April 2023, the river shows a slow recession and a low water level, corresponding to <0.5 m^3 s^{-1} of streamflow discharge or to <3.5 mm day^{-1}. This low winter streamflow is classically observed in many high-elevation catchments (>2200 m a.s.l.) (Schmid, 2024) and can result from groundwater baseflow, leaked glacier melt, and ground heat-induced snowmelt (Müller et al., 2024). The groundwater heads at borehole ID 4479 exhibit relatively stable and slow dynamics during the cold months. In contrast, the neighboring borehole ID 4478, which is 115 m away from borehole ID 4479, shows a strong recession and drop-down of the heads. These results underline the heterogeneous groundwater dynamics in high-elevation alpine catchments.

In May 2023, the river water level and both groundwater heads (IDs 4479 and 4478) were responsive to the early snowmelt and rainfall. Again, the groundwater borehole ID 4478 shows a much higher water level fluctuation (0.88 m) compared to the river gauge (0.24 m) and the other borehole ID 4479 (0.26 m). However, starting from glacier melt onset in June and in particular after glacier melt intensification in July (Fig.3b), the two boreholes show similar dynamics and responses to the total PEQ, in contrast to their different behaviors in winter and early summer. During the warm period, the river water level and the groundwater heads are all responsive to the snow and glacier melts and extreme rainfall events, such as those in August and September. Unlike the deep-circulated groundwater, which may show a long lag time in response to surface conditions, the shallow groundwater heads observed in this study increase as quickly as the river water level during the peak melts (e.g. May 2023) and extreme rainfall events in the headwater landscape. Overall, these results imply the needs of a precise partitioning of the liquid fluxes (rainfall, snow and glacier melt) between the surface and subsurface for achieving reliable hydrological simulations.

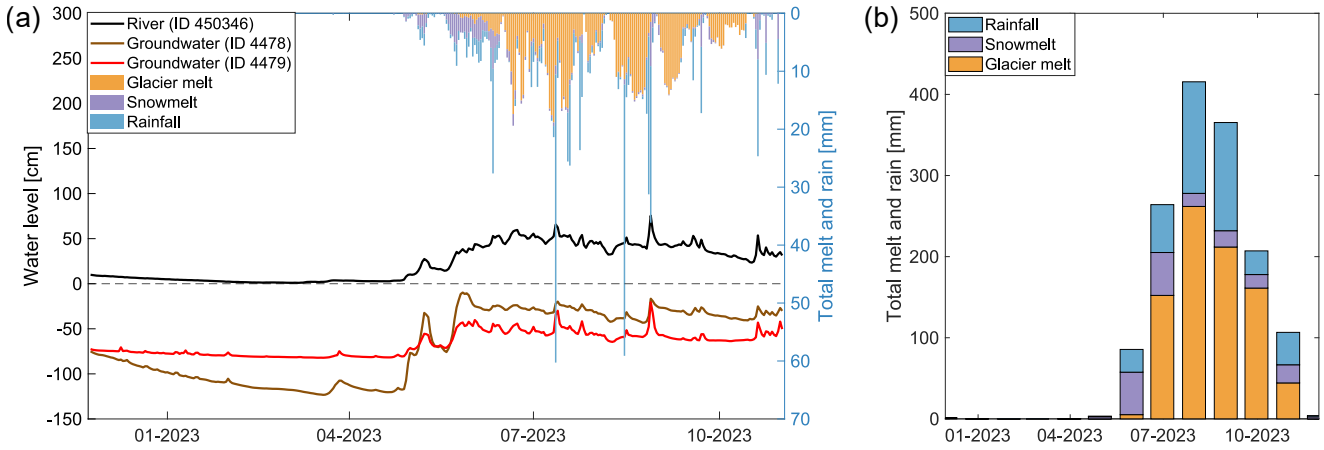

Figure 3. Hydrological response of the observed river water level and groundwater heads to the simulated total rainfall and meltwater from snow and glaciers between November 2022 and November 2023 in the glaciated headwater Subcatchment S8 (Fig.1) in the Martell Valley. (a) The observed daily river and groundwater level hydrographs and the simulated daily meltwater and rainfall in this subcatchment. The reference level for river water level is the riverbed, with zero indicating dry conditions. The reference level for groundwater is the ground surface. The station elevations are provided in Table 2. The black line denotes the river water level measured at the gauge Upper Plima (ID 450346) in cm day^{-1}. The red and brown lines denote the groundwater heads measured at the boreholes ID 4479 and ID 4478 in cm day^{-1}. The stacked bars on the top denote the simulated daily glacier melt, snowmelt, and rainfall in mm day^{-1}. (b) The simulated monthly total snowmelt, glacier melt, and rainfall in this subcatchment in mm $month^{-1}$. The yellow blocks denote the glacier melt, the purple blocks denote the snowmelt, and the blue blocks denote the rainfall.

5.3 Groundwater observation and simulation

Figure 4 shows the observed and simulated groundwater heads at five groundwater boreholes in the upper subcatchments S7 and S8 (Fig.1 and Tab.2) under two different model set-ups: with or without subsurface lateral flow allowed in the unsaturated zone in the model (called "interflow" in *WaSiM*). All observed boreholes measure the heads of unconfined shallow aquifers within the depth to water table (DTW) of 1.2 m. Our extensive parametric analyses show that the best simulations at all boreholes are achieved when the subsurface lateral flow is constrained to zero (Section S4 and Fig. S9-S13 in the Supplementary Materials). The Spearman's rank correlation coefficients (p-value < 0.001) of the best simulations against the observations are 0.89, 0.84, 0.41, 0.61, and 0.81 for borehole IDs 4479, 4478, 4476, 4473, and 4672 (Figs.4a-e). The MAE are 0.09, 0.31, 0.15, 0.18, 0.05 and the RMSE are 0.14, 0.41, 0.20, 0.21, 0.07. The NSE ranges between 0 and 0.4 though. By visual comparison, the simulations captured well the observed temporal dynamics, such as the head response to the early and peak snowmelt and to the extreme rainfall events. The magnitudes of water table fluctuations are also well modeled at most of the sites, except for borehole ID 4478 (Fig.4b) where the strong recession behavior in winter is challenging to simulate. When the subsurface lateral flow is allowed, the simulated groundwater hydrographs (blue and purple lines in Fig.4) underestimate the observed groundwater heads (black lines) and struggle to reproduce the observed temporal dynamics. These results provide new insights

into the potentially limited influence of subsurface lateral flow in streamflow generation in high-elevation headwater landscapes, such as in the Martell Valley that has a relatively dry climate and presence of shallow porous aquifers (groundwater heads within 1.2m depth). However, it is noteworthy that the piezometers were installed in a rather flat area in our study. The findings cannot be transposed as is to hillslope processes, which would require entire piezometer transects (extremely challenging to install in such environments) or distributed soil moisture sensing, for example, via Electrical Resistivity Tomography (ERT) (Müller et al., 2022) or via surface proxies (e.g., temporal occurrence of local saturation via repeated drone imagery) (Glaser et al., 2018).

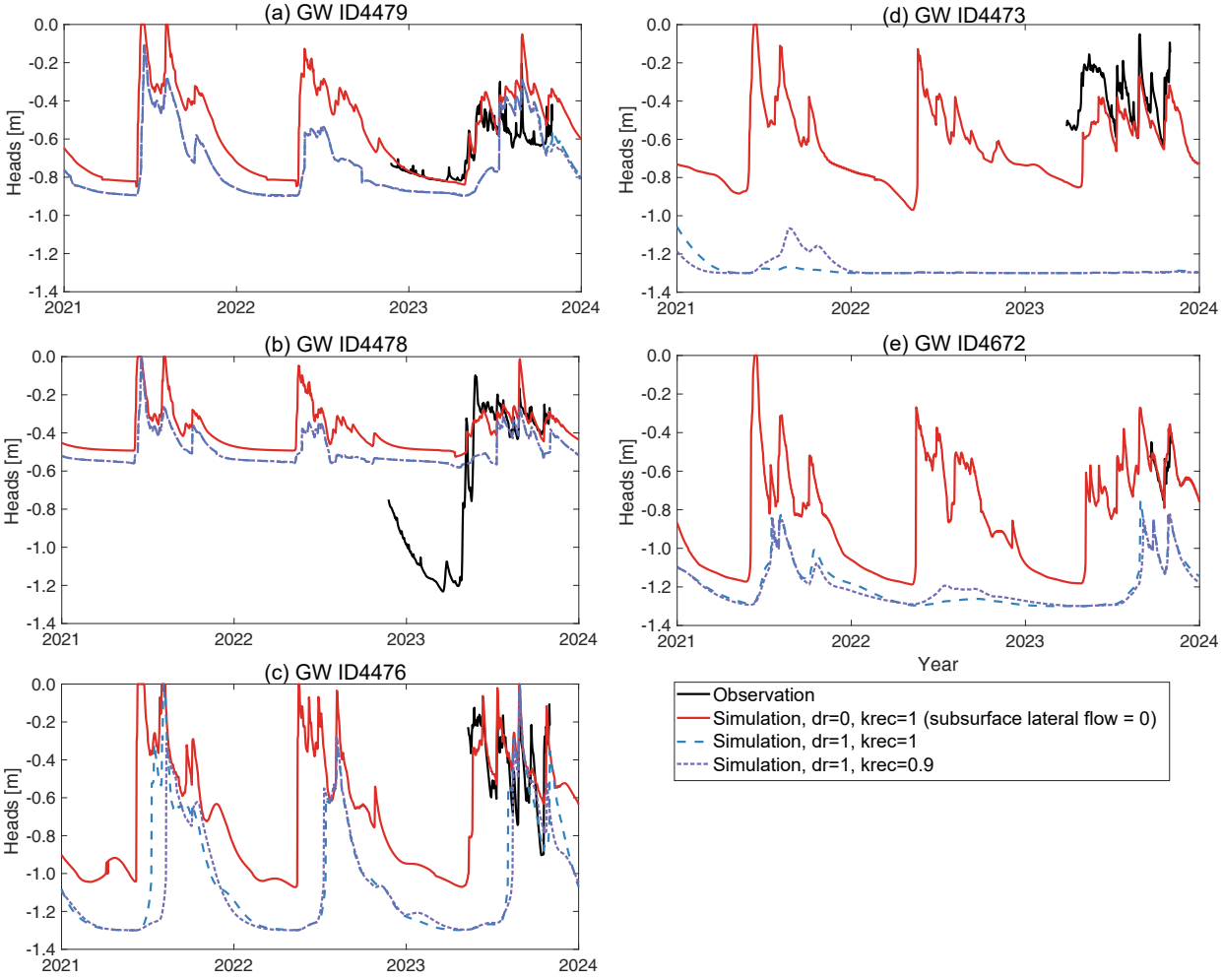

Figure 4. Observed and simulated groundwater heads at five piezometers in the upper headwater subcatchments S7 and S8 (Fig.1) with and without subsurface lateral flow allowed in the unsaturated zone. The groundwater heads are recorded as depth to water table (DWT) below the land surface. The black lines denote the observed hydrographs; the red lines denote the simulations with the subsurface lateral flow constrained to zero by setting the parameters of *dr*=0 and *krec*=1 in the *WaSiM* model; the blue and purple dashed lines denote the simulations with subsurface lateral flow allowed by slightly perturbing the *dr* and *krec* parameters.

To further investigate the reasons why the groundwater recession cannot be simulated at some locations in the model domain (e.g., bore ID 4478), we compute the Topographic Wetness Index (TWI, Eq.1) based on the DEM data - a key measure for understanding the topographic control on the catchment hydrological processes (Pourali et al., 2016; Beven and Kirkby, 1979). The TWI of the whole catchment ranges from 2.7 to 23.4, with an average of 6.0. The higher the TWI is, the wetter the corresponding model grid cell tends to be. We quantify the relationships between the TWI and the simulated annual mean

groundwater heads at the five boreholes and their neighboring grid cells. All locations show a positive relationship between these two variables (Fig. S3 in the Supplementary Materials).

Figures 5a-b show the spatial distribution of TWI in the upper headwater subcatchments S7-S9 (Fig.1) where the groundwater boreholes are installed. Boreholes ID 4479 and 4478 have the same local geology, land use, and soil properties, while a key difference between them is the TWI value: borehole ID 4479 has a TWI of 7.1 (Fig.5a) and its simulation shows an adequate performance in capturing the observed groundwater head variations (Fig.4a). In contrast, borehole ID 4478 is located within a flood plain (Fig.1) and has a TWI of 10.7 (Fig.5a), indicating that this area has higher potential to store water in the model; the topographic control hence contributes to explaining why the model struggles to release water at this location (Fig.4b). Other reasons for the deep winter groundwater recession observed at borehole ID 4478 could be the existence of local preferential flow paths or fractured rocks, which are still challenging to account for in fully-distributed hydrological models (Sivelle et al., 2025; Bronstert et al., 2023; Mazzilli et al., 2019).

Additionally, another key question is how reliable and representative the observed groundwater heads data at specific locations are for calibrating a comparable distributed model. In our study, the hydrograph of one borehole (ID 4479) can be simulated at the grid cell corresponding to the exact borehole coordinates (Figs.5a,c); but the model struggles to reproduce the observed groundwater head variations at the borehole ID 4478, which shows a nearly saturated subsurface and a very high TWI value in the model (Figs.5a,d). To overcome such difficulty, we compare the observations against the simulations not only at the grid cell containing the point observation but also at its neighboring cells (Figs.5c,d) to account for uncertainties related to the DEM data, model resolution and evolution of river networks. The ensemble of simulations shows the spatial and temporal groundwater heads dynamics near the observed locations (Fig.5d): some simulations indicate highly saturated subsurface, whereas the others capture well the observed fluctuations after the peak snowmelt. These results suggest that selecting borehole locations needs to be done very carefully, and that multiple neighbouring cells simulations should be considered for model evaluation. Moreover, some extent of mismatch between the real-world point observations and model grid-cell simulations is likely unavoidable. Further implications of these results on borehole installation and model evaluation are discussed in detail in Section 6.3.

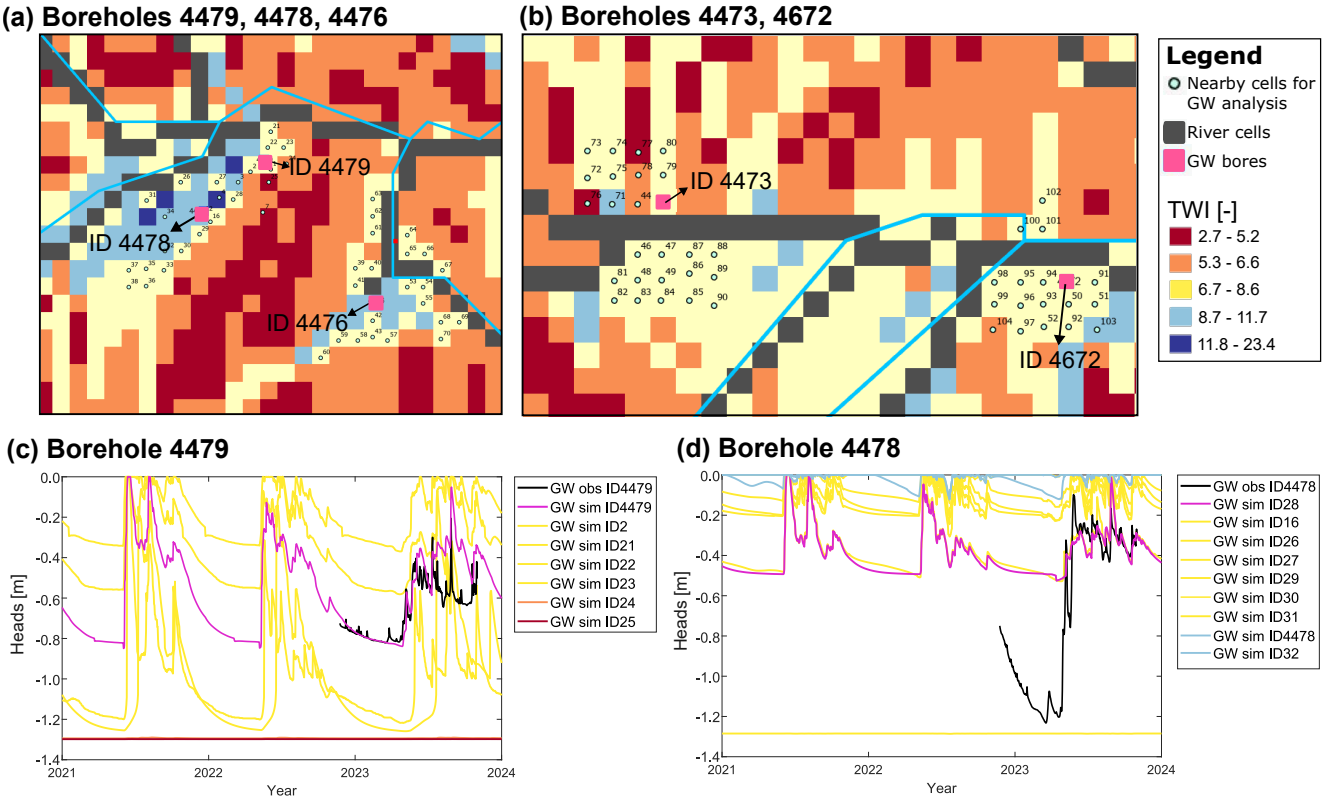

Figure 5. Spatial distribution of the Topographic Wetness Index (TWI) in the upper headwater subcatchments (S7–S9) and observed and simulated groundwater levels at monitored boreholes and nearby locations. (a–b) TWI maps (25 m × 25 m resolution) showing the five boreholes (IDs 4479, 4478, 4476, 4473, and 4672), observed river channels (blue), computed river networks from *Tanalys* (Schulla, 2024) (black), and nearby simulation locations (little dots with IDs). (c–d) Observed and simulated groundwater hydrographs (2021–2023) for boreholes 4479 and 4478. Black lines indicate observations, violet lines indicate the best-matching simulations (TWI ≈ 7), and the remaining colored lines represent simulations at nearby locations grouped by TWI category (red → yellow → blue). Plots of boreholes 4476, 4473, and 4672 are shown in Fig.S14 in the Supplementary Material.

5.4 River observation and simulation

Figure 6 shows the observed and simulated river discharge at three gauging stations (Fig.1). At the gauging station ID 450346 which is located in the upper headwater Subcatchment S8, the simulated and observed discharges have a Spearman's rank correlation coefficient of 0.90 (p-value < 0.001), an NSE of 0.76, an MAE of 0.24, and an RMSE of 0.40 (Fig.6a and Fig.S2c in Supplementary Materials). The model captures well the temporal dynamics of the observed discharge in terms of response timing to the early and peak snowmelt and extreme rainfall events, despite the slight underestimation of the very low winter discharge and occasional overestimation of the peak discharge in the extreme rainfall events.

At the official discharge station Plima located in the Subcatchment S7, the model captures well the observed temporal discharge dynamics (Spearman's rank correlation coefficient: 0.90 with a p-value < 0.001, NSE: 0.63, MAE: 1.05, RMSE: 1.49, see Fig.6b and Fig. S2b in Supplementary Materials). Nevertheless, the model struggles to fully capture the winter low-flow dynamics in some years. The observed winter low flow has an annual mean of 0.59 $m^3\ s^{-1}$ or 2.0 mm day^{-1} (between December and March from 2018 to 2024) given the subcatchments area of 25.3 km^2, which is not uncommon for corresponding elevations (>2400 m a.s.l.). But there appears to be more measurable winter low flow in 2019 and 2020 which are not captured by the model. The measured quick drop in winter discharge in 2021 was more likely due to instrument errors under frozen conditions (e.g., the sensor is frozen during low temperatures). Similar to station ID 450346, the model occasionally overestimates the high flow rates. This could partly be attributed to the uncertainty in the observed discharge, which is computed from observed river water levels with a rating curve (Hofmeister et al., 2023b) where the high flows are typically underrepresented in the measurements (Di Baldassarre and Montanari, 2009).

The catchment outlet is located in the downstream Subcatchment S2. Despite the irregular observations at this station (ID 450499), the simulation captures the observed discharge dynamics (Spearman's rank correlation coefficient: 0.87 with a p-value < 0.001, NSE: 0.50, MAE: 1.50, RMSE: 1.89, see Fig.6c and Fig. S2a in Supplementary Materials). The relatively lower model performance at this downstream subcatchment (S2) compared to the other two subcatchments (S7, S8) could be because the majority of the hydrological stations that are used to calibrate the model parameters are located in the upper subcatchments. We cannot further comment on winter model performance for this station due to little reference data.

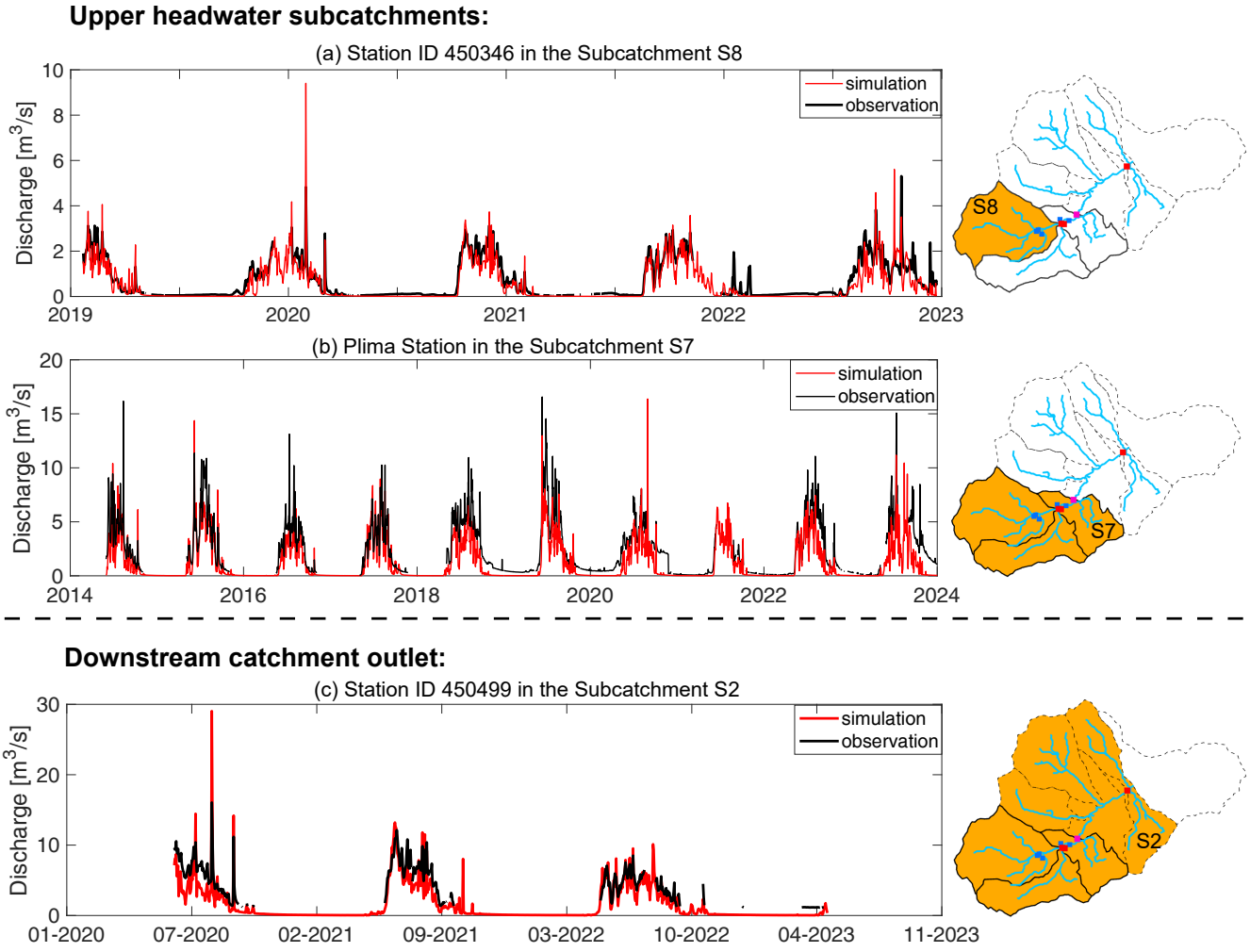

Figure 6. Observed and simulated river discharge at (a) Station ID 450346 located in the upper headwater Subcatchment S8, (b) Plima Station located in the upper headwater Subcatchment S7, and (c) Station ID 450499 located in the Subcatchment S2 and measuring the downstream catchment outlet. The black lines denote the observations, and the red lines denote the simulations. The drainage area of each gauging station is marked in orange in the maps on the right. The dark blue dots denote the groundwater piezometers; the red dots denote the river gauges. Details of the hydro(geo)logical stations are provided in Figure 1 and Table 2.

Figure 7 shows the simulated surface runoff ("direct flow" in the model), groundwater baseflow, and the proportion of baseflow in the streamflow (i.e., baseflow divided by the sum of direct flow and baseflow) in the upper headwater subcatchments (S7, S8) and the downstream catchment outlet (Fig.1). Following calibration against observed groundwater heads at the five piezometers, the subsurface lateral flow is constrained to zero (Section S4 and Figures S9-S13 in the Supplementary Materials). Both direct flow and baseflow exhibit interannual and seasonal variability and respond quickly to the peak snowmelt (Figs.7a-f). The direct flow shows to dominate the total discharge in all subcatchments (Figs.7a-c). The relative low baseflow might

be attributed to the piezometers being installed exclusively in the upper headwater subcatchments with shallow soil formation (Ramskogler et al., 2023), where the baseflow contribution is likely smaller than the area with thick soil profile such as the valley floor (see the conceptual diagram of Figure 1 in the work of van Tiel et al. (2024)). Besides this, a small hydraulic gradient between groundwater table and river was observed in the field (i.e., shallow river depths $<$10 cm and river width $<$2 m in the flat flood plain where the hydro(geo)logical stations are installed, see Fig.1d), leading to lower groundwater exfiltration to the river. Furthermore, given that only shallow groundwater heads were measured in this study, the quantified baseflow primarily represents the contribution from unconfined shallow aquifers. Deep groundwater contributions are not modeled due to data limitations but are expected to be more significant downstream, where Quaternary valley sediments offer higher potential for deep groundwater storage. The estimated downstream baseflow (Fig.7i) may hence contain higher uncertainty due to lack of deep groundwater observations and need to be interpreted with caution.

Nevertheless, excluding deep groundwater from the model does not compromise the model's merit in the headwater catchment scale. Results show that shallow aquifers contribute significantly to sustaining winter streamflow: up to 30-40% in the upper headwater subcatchments (S7, S8) - similar magnitude to the proglacial outwash plain in the Swiss Alps (Fig.13 in the work of Müller et al. (2022)). During the snow accumulation period, the model reproduces the observed groundwater level decline reasonably well for borehole ID 4479 but underestimates it for borehole ID 4478 (Figs.4a,b). It implies that shallow aquifers described in the model may locally overestimate the storage (Figs.4ab). However, the shallow piezometers do not fall dry, and the experimental evidence does not preclude connectivity between the shallow aquifer and the river during this period. Consequently, winter baseflow cannot be attributed solely to deeper flow paths. Besides that, the stable water isotope analyses from November 2022 and November 2023 show consistent values between groundwater and river water during the onset of low-flow season (e.g., δ^2H: -94, -96, -90‰at boreholes ID 4478, ID 4479, and stream gauge ID 450346 in November 2022; -85‰at both borehole ID 4478 and the stream gauge ID 450346 in November 2023), despite the uncertainty due to a limited number of water samples. These results further support the hypothesis of a tight connection between the shallow aquifer and the river during winter. Deep groundwater processes were not directly constrained in this study because groundwater observations and model representations were limited to the shallow aquifer. However, we consider it unlikely that deeply circulating groundwater from the hillslopes of the proglacial outwash plain provides a substantial contribution to the stream network in the upper headwater floodplain. Such deeper groundwater contributions are more likely to occur in the valley floor, where longer flow paths may connect groundwater with the river network (Fig.1b in the work of van Tiel et al. (2024)).

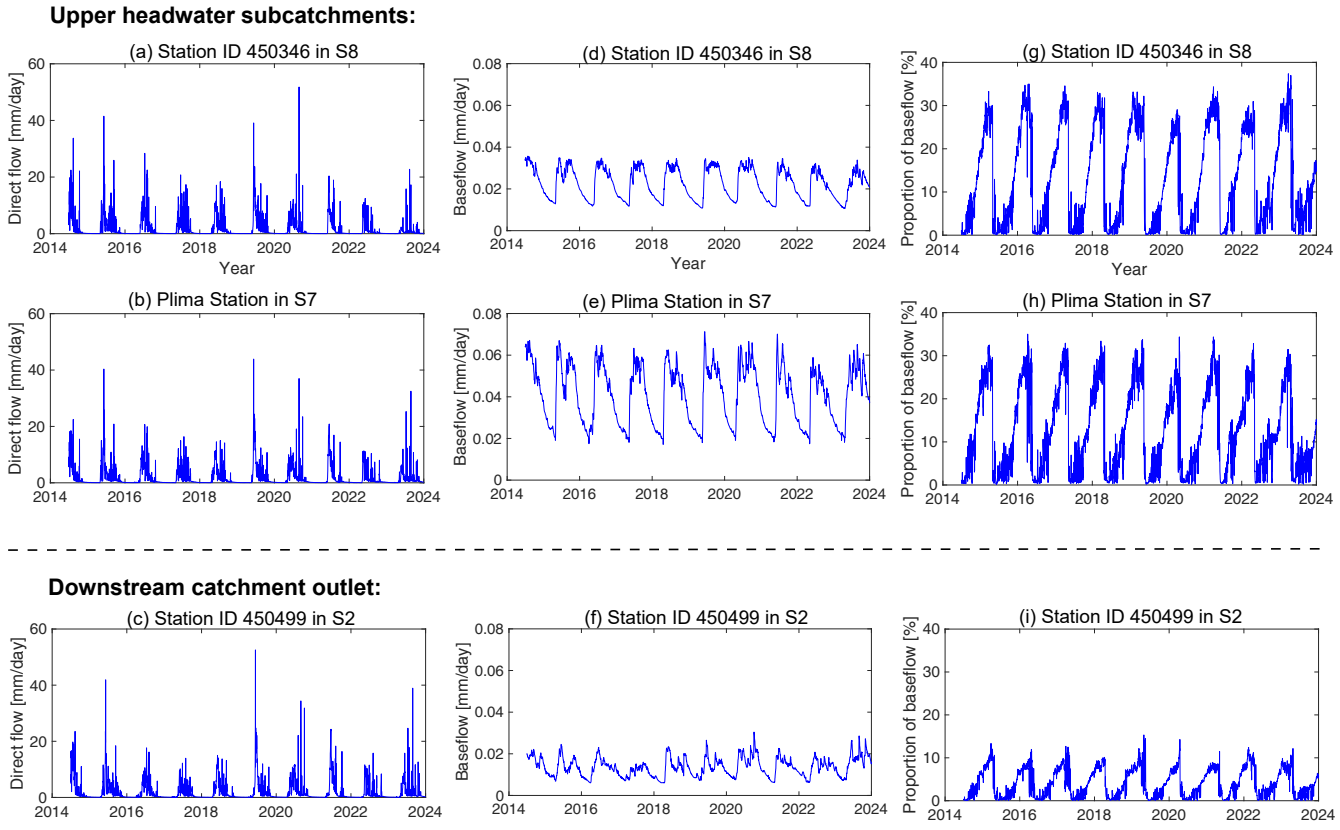

Figure 7. Simulated surface runoff (direct flow), baseflow, and the proportion of baseflow in the streamflow in the upper headwater subcatchments (S7, S8) and the downstream catchment outlet (located in Subcatchment S2). (a-c) direct flow in mm day^{-1}, (d-f) baseflow in mm day^{-1}, (g-i) the proportion of baseflow [%] in the streamflow (i.e., baseflow divided by the sum of direct flow and baseflow). Note that following calibration to the observed groundwater heads, the subsurface lateral flow was constrained to zero. The locations of the subcatchments are shown in Figure 1.

5.5 Spatial analysis of key hydrological dynamics

Figures 8 and 9 show the simulated key hydrological spatial dynamics of monthly percolation, groundwater recharge, groundwater heads, groundwater exfiltration to the river, and river infiltration into the groundwater in February (lowest flow), June (peak snowmelt), September, and December (low flow) 2023. The regions marked with dashed squares (i.e., Subcatchments S7-9 in Figure 1) have the majority of hydro(geo)logical stations installed, with which the model was calibrated. Percolation represents the vertical free drainage into the groundwater. The groundwater recharge is calculated as the water balance between the vertical and horizontal inflow and outflow for each grid cell. During the low-flow period in February 2023, percolation and groundwater recharge were minimal across the catchment. The groundwater heads lay within 1 m depth near the river networks and the Zufritt lake in winter, whereas they dropped beyond the model's lower boundary in other regions (Fig.8). During the

peak snowmelt period around May and June, percolation reached its annual maximum, leading to widespread groundwater recharge across the catchment—except at very high elevations and in steep terrain (Fig.8). Consequently, groundwater levels rose, particularly near river channels and in valley bottoms. The percolation, recharge, and groundwater heads remained at a high level until September 2023, when the total liquid input (rainfall, snowmelt, glacier melt) into the catchment was still high (Fig.3b). After that, they gradually turned to a low state in December 2023.

Figure 9 illustrates the seasonal spatial dynamics of groundwater-river interactions. Groundwater consistently exfiltrates to the river throughout the year in the main river channels, meaning these reaches behave as "gaining streams", with exfiltration rates decreasing as elevation increases. Groundwater is found to recharge the river channels even at the highest elevations during peak snowmelt (in June), when the active stream network is fully developed and gaining-stream conditions extend across the network. In contrast, in February, groundwater only recharges the main river channels, and gaining-stream conditions become spatially restricted as groundwater exfiltration becomes disconnected in river networks at higher elevations, where parts of the stream network are inactive. This is in line with the typically observed retraction of the active stream network during winter months at comparable elevations (Michel et al., 2022; Paillex et al., 2020). Unlike groundwater exfiltration, river infiltration into groundwater (i.e., "losing-stream" conditions) occurs only in the main river channels at the valley bottom. This is because baseflow (groundwater exfiltration) can occur at any stream network grid cell adjacent to a groundwater cell, while river infiltration into groundwater is limited to the groundwater cells adjacent to the main river channels in *WaSiM*. This setup reflects the assumption in the model that flow gradient is usually directed from groundwater to rivers in the headwater landscapes, with reversal of this gradient —and thus the formation of losing streams— only possible under large external inflows to the routing channels (Schulla, 2024). Overall, these findings demonstrate the model's capacity to represent the spatial and temporal patterns of hydrological changes in great detail, including the timing and location of groundwater recharge as well as the seasonal interactions between groundwater and river systems.

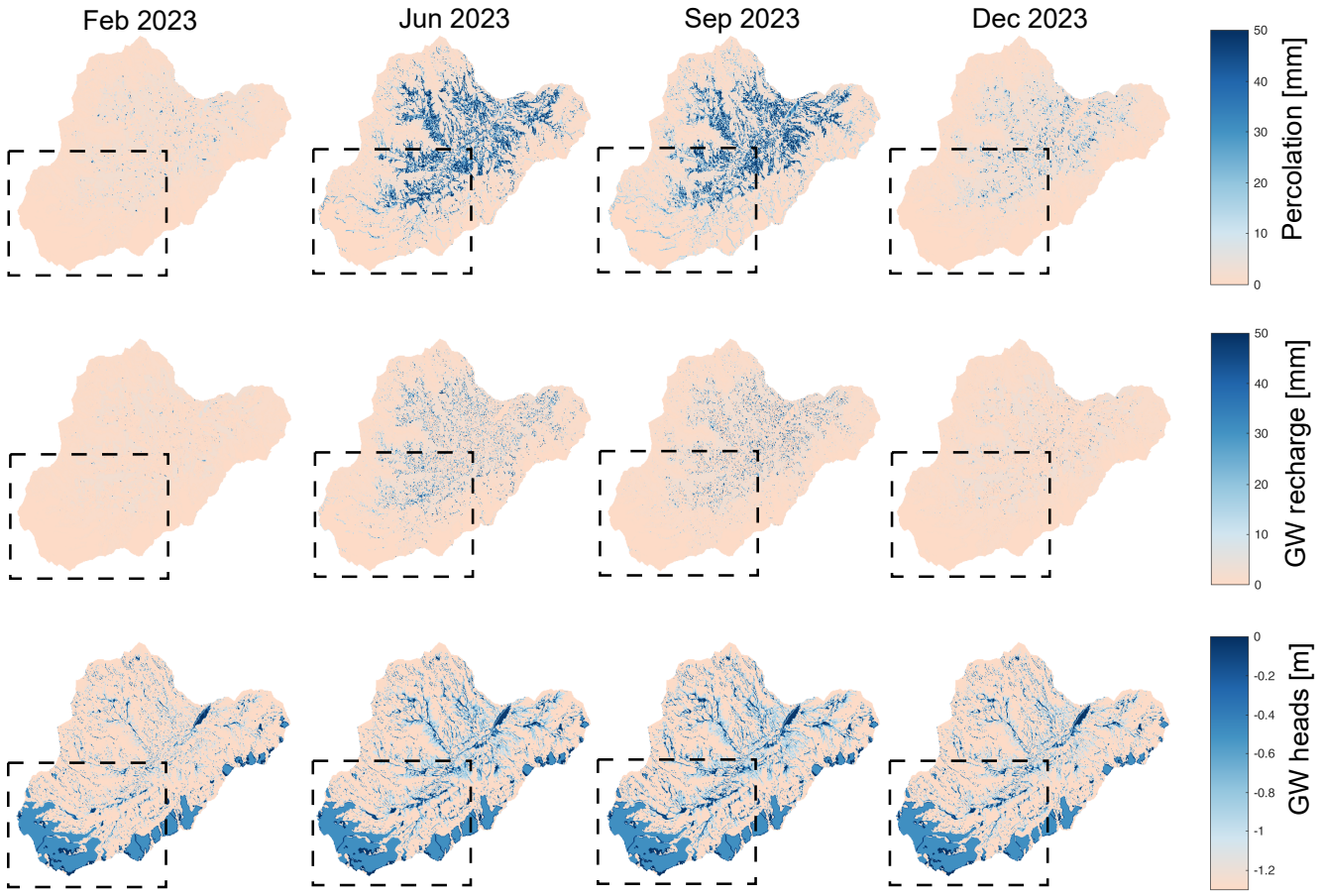

Figure 8. Spatial distribution of simulated monthly percolation, groundwater recharge, and groundwater heads (in depth to water table) in the Martell Valley in February, June, September, and December 2023. The "Percolation" is defined as the vertical flux into the groundwater system, while the "groundwater recharge" is defined as the net change of groundwater storage after balancing both vertical and horizontal inflow and outflow in the *WaSiM* model. The dashed squares indicate the area containing the majority of installed hydro(geo)logical stations (i.e., Subcatchments S7-9 in Figure 1), where the results have higher confidence.

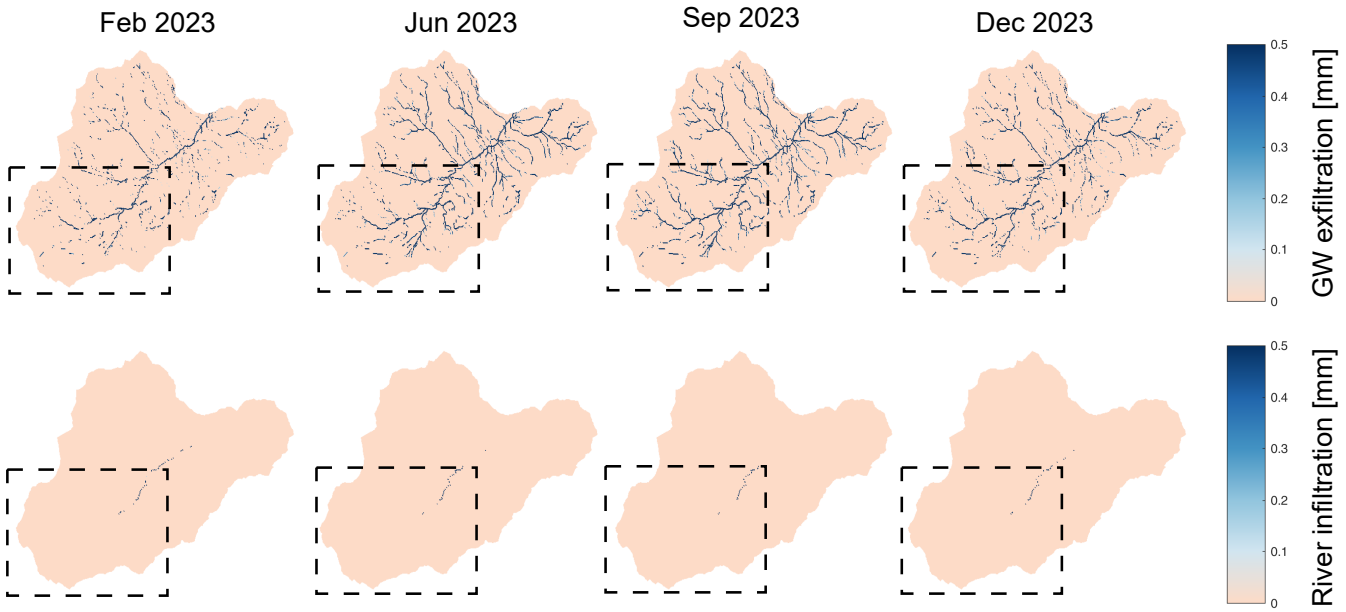

Figure 9. Interactions between groundwater and river networks (groundwater exfiltration to the river, river infiltration into groundwater) in the Martell Valley in February, June, September, and December 2023. The dashed squares indicate the area containing the majority of installed hydro(geo)logical stations (i.e., Subcatchments S7-9 in Figure 1), where the results have higher confidence.

6 Discussion

6.1 Comparison with existing modeling efforts

Our results can be compared most directly with those of Thornton et al. (2022), who externally coupled *WaSiM* (surface module) (Schulla, 2024, 1997) and *HydroGeoSphere* (HGS, subsurface module) (Aquanty, 2016) to investigate groundwater–surface water interactions in a high Alpine catchment. Thornton et al. (2022) emphasized the importance of the near-surface soil zone for partitioning rainfall and meltwater between surface and subsurface pathways. By adopting a fully-integrated modeling approach, our results support the importance of this partitioning process, by including groundwater observations to provide additional constraints on the modelled water fluxes. However, an unexpected outcome of our study is that the best simulation agreement with observed groundwater levels and streamflow was obtained when subsurface lateral flow was switched off after exploring a large ensemble of Monte-Carlo simulations (Figs.4,6 and Figs.S9-13 in Supplementary Material). Given the limited number of integrated hydrological modeling studies in high-elevation glaciated catchments, additional applications using alternative model structures, independent observations, and event-scale analyses are needed to determine whether the reduced role of subsurface lateral flow identified here is site-specific or reflects a more general characteristic of high-elevation headwater environments.

Our findings also contribute to the growing body of work evaluating groundwater–cryosphere interactions using groundwater observations. Thornton et al. (2022) and Aubry-Wake et al. (2024) demonstrated the value of shallow groundwater level data for constraining hydrological processes in high Alpine catchments, while van Tiel et al. (2024) highlighted the broader challenges associated with representing groundwater dynamics in cryosphere-dominated environments. Similar to these studies, our study shows that the inclusion of groundwater observations provided information that could not be inferred from streamflow alone. In particular, the groundwater data indicate that satisfactory streamflow simulations do not necessarily imply a realistic representation of subsurface processes. This finding reinforces the importance of multi-variable evaluation frameworks when assessing hydrological model performance.

Compared with the externally coupled *WaSiM–HGS* framework of Thornton et al. (2022), the fully-integrated *WaSiM* model adopted here reproduced both shallow groundwater dynamics and streamflow with comparatively limited hydrogeological information. However, this result should be interpreted cautiously. WaSiM imposes structural simplifications, including the requirement that the lower boundary of the soil profile coincides with the lower boundary of the aquifer, which may limit its applicability in catchments with more complex subsurface architecture. Conversely, the physically more detailed three dimensional HGS model requires a substantially greater degree of calibration effort and (hydro)geological data, which are often unavailable in high-elevation glacierized catchments. The contrasting performance of the two approaches (e.g., Figs. 3 and 4 in the works of Thornton et al. (2022) compared with Figs. 4 and 6 in this work) suggests that intermediate-complexity integrated models (e.g., WaSiM) may provide a useful compromise for process-based modelling in data-limited high Alpine environments.

Finally, our results are consistent with recent studies that advocate incorporating subsurface information into model calibration and evaluation (Liu et al., 2025; Talbot et al., 2024). In catchments where groundwater observations are unavailable, groundwater recharge estimates have been proposed as alternative constraints for improving the representation of surface–subsurface interactions (Liu et al., 2025). Although such estimates are generally associated with larger uncertainties than groundwater level observations, they contribute to improved quantification of internal hydrological fluxes and to reducing equifinality during model calibration. Together, these studies and our results demonstrate that incorporating subsurface information is essential for evaluating model realism and improving process understanding in glacierized catchments.

6.2 Insights from fully-integrated hydrological modeling

The fully-integrated surface-subsurface hydrological model enables detailed exploration of hydrological dynamics and interactions between the surface and subsurface in alpine environments, providing enhanced understanding of hydrological processes. The observations of shallow groundwater heads reveal their rapid responses to peak melts and extreme rainfall events, with dynamics comparable to streamflow fluctuations (Fig.3). This rapid response is indicative of runoff generation via groundwater feedback mechanisms (Ala-aho et al., 2017; Appels et al., 2017), which have been rarely captured in conventional hydrological models. Traditional conceptual models, typically relying on simplified linear subsurface representations, fail to reproduce such behavior (Horton et al., 2022). Even physically based models employing Richards' equation may not adequately resolve these dynamics without incorporating additional mechanisms, such as preferential flow pathways like the fractured substrates

(Sivelle et al., 2025; Bronstert et al., 2023; Mazzilli et al., 2019), piston-flow dynamics (Wang et al., 2018; Paniconi and Putti, 2015), or explicitly accounting for saturation-area effects such as in the dynamic Topmodel approach as implemented in the DECIPHeR model (Coxon et al., 2019). These findings underscore the need for improved subsurface parameterizations to better represent rapid shallow groundwater–surface water interactions in high-alpine hydrological modeling.

Despite the observational and modeling challenges associated with high-elevation environments, this study demonstrates how fully-integrated hydrological models constrained by multiple hydro(geo)logical observations, particularly groundwater levels, can provide new insights into alpine hydrological processes. A key outcome of our analysis is that the behavioral model simulation consistently indicates a limited contribution of subsurface lateral flow to streamflow generation in the upper headwater catchment. Under the simulated conditions, streamflow can be adequately explained by groundwater baseflow and surface runoff, while subsurface lateral flow (or "interflow", in the unsaturated zone) is not needed by the model to explain the observed dynamics, while considering both the river and the aquifer systems. This result does not necessarily imply that the subsurface lateral flow is absent. Rather, the rapid subsurface lateral flow (i.e., the associated response dynamic) is not needed to explain catchment-scale daily discharge and local-scale groundwater dynamics. The result suggests that the contribution of subsurface lateral flow to catchment-scale daily discharge may be smaller than commonly assumed in glaciated high Alpine environment, which is consistent with the conceptual description of hydrological flow processes in high Alpine landscapes in the recent work of van Tiel et al. (2024) (Fig.1), compatible with the observation discussed by Hayashi (2019), and in line with the review-based discussion that alpine aquifer systems can have highly dynamic, hydraulically active zones that contribute to streamflow (McGuire et al., 2024; Somers and McKenzie, 2020).

It is noteworthy that our conclusion refers specifically to the modeled dominant contributions to river discharge at the daily catchment scale. The quantified contribution of each flow component is not based on direct measurement but emerges from the ensemble of hydrological simulations used for model calibration, which was evaluated against both groundwater level and river discharge observations. Within the current model structure and parameterization, explicitly simulated subsurface lateral flow (interflow) is not needed and even leads to a poorer reproduction of the observed streamflow and groundwater dynamics (Fig. 4 and Figs. S9-S13 in the Supplementary Material). This could be a model artefact, primarily because of model complexity. However, our systematic testing suggests that this explanation is unlikely (see Figs. S9-S13 in the Supplementary Material).

Based on the physical characteristics, the alpine environments are characterised by steep slopes and are assumed to have strong contrasts in subsurface hydraulic conductivity - conditions that tend to promote subsurface lateral flow (McGuire et al., 2024). However, our study site is also characterized with shallow soils, i.e., limited storage potential, that favor percolation to aquifers which in turn can be highly connected to the stream network and show high dynamics (Hayashi, 2019). In addition, recent evidence of high erosion potential near the Zufallferner within the study site (Altmann et al., 2025) provides indirect support for the importance of surface-dominated flow pathways during rainfall and melt events. Our model-based conclusion is hence a plausible representation of high alpine streamflow generation dynamics, in particular given that it reproduces streamflow (flux) and groundwater dynamics (storage).

As reviewed by McGuire et al. (2024), observing subsurface lateral flow (interflow) remains a considerable challenge. The limited availability of observational data has substantially constrained our ability to accurately predict interflow and quantify

its contribution to streamflow across diverse hydrological settings. In the future, more field campaigns should be designed to challenge this result, in particular based on tracer observations (McGuire et al., 2024; Xie et al., 2024). Furthermore, from a modelling perspective, we show the importance of calibrating any model against observations of streamflow and storage dynamics to avoid representing the observed streamflow dynamics with processes that might not be at play.

6.3 Recommendations on groundwater piezometer installation and evaluation

By calibrating the hydrological model's subsurface module to the observed groundwater heads, we found that the model performed well at some sites but struggled at others, particularly at borehole ID 4478, where the model failed to reproduce the recession observed in winter (Fig.4b). To explore this further, we calculated the Topographic Wetness Index (TWI) and found that the TWI at this location (10.7) is significantly higher than the catchment average (6.0), suggesting that the model's inability to drain the subsurface is linked to local topographic conditions. To address such challenges in high-elevation hydrological modeling in the future, we suggest the following:

(i) We recommend first computing the TWI (Eq. 1) for the study catchment by using the DEM data and the grid cell resolution that will be used for subsequent hydrological modeling. The TWI values can then be used to inform the selection of groundwater piezometer locations, in conjunction with additional field information and expert knowledge. The spatial resolution of the TWI should match the model resolution which should be chosen based on research objectives and site-specific characteristics, such as elevation gradients and slopes. In this study, we tested model resolutions of 20×20m, 25×25m, 50×50m, and 100×100m, and we ultimately selected 25×25m by balancing the trade-off between computational efficiency and topographic complexity of the study site. Using TWI to pre-select borehole locations helps avoid areas with extreme wetness or dryness where the model may struggle to accurately simulate groundwater dynamics. Given the high resolution of input data required for complex models in rugged terrain, the fully-distributed model is sensitive to errors in the observational data, such as borehole coordinates and DEM accuracy. Since correcting fine-scale DEM errors is challenging, installing the piezometers at locations that are promising for comparison with the model, i.e., by adapting the modeling task to the DEM data uncertainty, can potentially help improve groundwater simulations.

(ii) Grid-cell-scale simulated groundwater levels might reliably represent larger-scale average groundwater dynamics despite not agreeing with local observed groundwater levels. This could be analogous to snow modeling where the simulated snow grid-scale heights may not be comparable to in-situ observations at the exact station location but still represent adequate performance in the catchment scale (Dong, 2018). Due to the intrinsic uncertainty in observation and modeling, we recommend to calibrate and evaluate the model performance not only to the simulated groundwater hydrographs at the exact location but also to consider those at their neighboring grid cells.

6.4 Limitations

This study is among the first fully-integrated and fully-distributed hydrological modeling for a comparable high alpine glaciated catchment, with a multi-signal calibration approach including groundwater level observations. The model is calibrated based on expert knowledge, systematic and step-by-step hand-tuning, and Monte-Carlo parametric analysis (Section S3 and S4 in

the Supplementary Materials). Unfortunately, the automatic calibration is computationally prohibitive and the number of parameters to calibrate in the model would not align with the amount of available reference data for such an automatic calibration. Considering the parameter uncertainty, the retained calibration in this study corresponds to a physically reasonable parameterization but not to any sort of optimal parameterization. To overcome the shortcomings of calibration (e.g., inefficiency, subjective parameter choices), we tackle this challenge by following a standardized approach outlined in Section 4.4.2. Overall, the detailed model evaluations module by module with the observed data (SWE, annual glacier mass balance, river discharge, groundwater heads) show reasonable model performance; the relative contribution of baseflow in streamflow and the temporal and spatial surface water-groundwater interactions reconfirmed the simulated system dynamics (relative changes) to be plausible and reasonable.

As the subsurface properties are calibrated against the observed groundwater heads in the upper subcatchments, the simulated baseflow in the downstream may contain higher uncertainty. Likely attributed to the same geological units and similar water fluctuation depths at all piezometers (Fig.1), many calibrated subsurface parameters are found to be identical at the observed locations (Tab.4). We include the essential subsurface heterogeneity by calibrating hydraulic conductivity for each soil layer (vertical heterogeneity) and each soil type (horizontal heterogeneity), primarily because obtaining effective (calibrated) hydraulic conductivity is a prerequisite for a hydrologic model to reliably simulate observed streamflow. It is still a key challenge in physics-based models, which often rely on pedotransfer functions to estimate hydraulic conductivity (Paschalis et al., 2022). Assigning spatially heterogeneous subsurface properties in the ungauged area involves numerous assumptions. We therefore applied a conservative approach to ensure the essential subsurface heterogeneity. Heterogeneities occurring at fine scale (e.g., soil properties and varying depths) are challenging to characterize, as demonstrated by the vast literature in stochastic hydrogeology, starting from the detailed investigation of the famous sites of Borden and Columbus (Rehfeldt et al., 1992; Woodbury and Sudicky, 1991). Detailed exploration of the impact of spatially variable subsurface parameters is beyond the scope of this study.

As pointed out by van Tiel et al. (2024), it is challenging to describe processes controlling cryosphere-groundwater interactions in high-alpine catchments due to a lack of observations and modeling challenges. The deep aquifers might exist in the Quaternary sediments in part of the catchment, likely in the downstream valley floors. However, details of deep aquifers are vastly unavailable in alpine landscapes. Remote sensing data offer an option to estimate groundwater storage changes. We could think of GRACE satellite data (Liu et al., 2022; Xiang et al., 2016), but the low spatial resolution (hundreds of kilometers) is often too coarse for high-elevation glaciated catchments characterized by an area commonly smaller than 100 km^2 (e.g. in Europe), leading to high uncertainty in the estimated groundwater storage and changes and challenge to be adopted in fully-distributed hydrological models. Another limitation of satellite-based gravimetry is the superimposition of gravity changes in glaciated high mountains; for example, the changes in mass are combined impacts due to glacier melt, seasonal snow cover, and fluctuations in subsurface storage (Voigt et al., 2021). Therefore, in-situ deep groundwater level data are still required to validate the satellite data and to calibrate the fully-integrated hydrological models. By adopting integrated hydrological modeling, our research aim is to contribute to new understandings of how water partitioning is shaped by spatial and temporal surface water-groundwater interactions, especially the near (sub)surface hydrological processes.

Additionally, we acknowledge the hydrological simulation uncertainty due to the rather coarse spatial resolution of the adopted soil dataset (HWSD, 1km × 1km), which is primarily limited by the sparse field observations available in the high mountain environments. A slightly higher resolution of global soil product (e.g., SoliGrids in 250m × 250m) (Batjes et al., 2020) may not necessarily improve the simulations significantly because of limited field observations in the high elevations. In this study, we used the land use map (e.g., the presence of rocks, forests, and grasslands) to evaluate and modify the soil type data, as another layer of validation of data quality. The HWSD product is adopted in this study as it remains widely used in regional modeling (Trinh et al., 2018; Bosco et al., 2015; Livneh et al., 2015) and it has harmonized and internally consistent soil attributes across broad spatial extents.

In the highest part of the Martell Valley, permafrost might exist, where water from snowmelt, ice melt, and rainfall may undergo multiple freeze-thaw cycles under periglacial conditions before entering the aquifers and being discharged (Brighenti et al., 2023; Reato et al., 2022). However, permafrost-related freezing and thawing processes are not included in our simulations because the corresponding *WaSiM* parameters could not be reliably constrained without soil temperature observations. Although the model can simulate soil freezing and thawing, spatially-distributed soil temperature measurements are needed for calibration and evaluation of freezing and thawing depths, and such observations are rarely available in high-elevation catchments. We acknowledge that in regions with significant glacier and permafrost cover, neglecting these effects may introduce uncertainty in characterizing groundwater components, with potential shortcomings in snow and ice melt estimates.

7 Conclusions

In this study, we simulate the complex surface-subsurface hydrological processes and quantify the interactions between the key hydrological components (snowmelt, glacier melt, river discharge, groundwater) in a high-elevation glaciated catchment (Martell Valley), with the fully-integrated and fully-distributed hydrological model *WaSiM*. Results show that the shallow groundwater heads respond as quickly as streamflow to peak snowmelt and extreme rainfall events (Fig.3). As this quick groundwater response is rarely expected and simulated, it highlights the need for improved subsurface parametrization in high-alpine hydrological modeling. By incorporating shallow groundwater head observations into the multi-signal calibration, we found, unexpectedly, that subsurface lateral flow in the unsaturated zone contributes limitedly to streamflow generation in the study site (Fig.4), suggesting that groundwater flow, in combination with surface runoff, is dynamic enough to explain the observed daily streamflow dynamics in the computational settings. This study also underscores the crucial contribution of winter groundwater baseflow to streamflow in high-elevation alpine landscapes and reveals the dynamic temporal-spatial interactions between surface water and groundwater.

Furthermore, the results underline the challenges of integrating point-scale groundwater observations into the calibration of a fully-distributed hydrological model. To overcome this challenge, we recommend to anticipate model-resolution effects before installing piezometers in the field, to avoid local effects that can reasonably not be reproduced by the model. As in the present work, a key information for the choice of piezometers placement is the Topographic Wetness Index (TWI), whose values indicate the extremely wet and dry model-grid cells that should be avoided for reference observations. Additionally, we

recommend evaluating the simulated groundwater hydrographs with those from a range of neighboring grid cells close to the observed locations. This is a simple yet efficient method to address intrinsic observational and modeling uncertainties.

As the first physics-based, fully-distributed, and fully-integrated surface-subsurface hydrological modeling study in the high-elevation glaciated environment, the achieved new insights on hydrological processes should be further tested and confirmed in other high Alpine settings. The insights from this study are most likely applicable to the mountain ranges with similar climatic, geological, and landscape settings and the sites with similar subsurface properties, such as the central European Alps, Scandinavian Mountains, and Canadian Rockies (Welch and Shaw, 2025; Stutenbecker et al., 2016; Ebbing et al., 2012). The high-elevation headwater catchments in these non-carbonate mountain ranges share key characteristics, where Quaternary sediments host shallow aquifers, impermeable bedrock restricts deep percolation, and subsurface lateral flow can be potentially limited. These are opposed to settings with distinct subsurface properties, e.g. the Hindu Kush Himalaya or with very different climatic settings, e.g. the Andean Alps (Owen and Dortch, 2014; Duncan et al., 2003). Future investigations can refer to the demonstrated workflow and recommendations (Sec. 6.3) and potentially overcome the limitations (Sec. 6.4). Such global case modeling and intercomparison contribute to a holistic understanding of hydrological processes in high Alpine environments.

Code availability. A compiled version of the hydrological model *WaSiM* is available at http://www.wasim.ch/en/ (no source code available) (Schulla, 2024). The ΔSnow model (v1.0.2) used for transforming the snow height data to snow water equivalent is accessible in the R package "*nixmass*" (Winkler et al., 2021). The MATLAB function *mannkendall* (v1.0.0) is adopted for quantifying the temporal trends of the hydrological variables (Collaud Coen and Vogt, 2021; Collaud Coen et al., 2020).

Data availability. The hydro-meteorological data used in this study are available in Zenodo (https://doi.org/10.5281/zenodo.21246869). The river gauge ID 450499 was destroyed during the extreme flooding events between 12 July and 9 August 2023. The discharge data of the official Plima Station are obtained from the Autonomous Province of Bozen (Bolzano) - South Tyrol. The observed climate data at Station Langenferner are obtained from the Institute of Atmospheric and Cryospheric Sciences of the University of Innsbruck in Austria. The data at Station Careser are obtained from Meteo Trentino in Italy (http://storico.meteotrentino.it/web.htm?ppbm=T0065&rs&1&df). Other station data are obtained from the Autonomous Province of Bolzano, South Tyrol in Italy. The Digital Elevation Model (DEM) data in 2006 are obtained from Province of Bolzano (di Bolzano Alto Adige, 2006). The land use and land cover data of the site in 2018 are obtained from the Corine Land Cover Data Center (CORINE Land Cover, 2018). The soil profile and attributes in 2018 are extracted from the Harmonized World Soil Database (version 2.0) (FAO & IIASA, 2023; Ramskogler et al., 2023). The geological information of the site is obtained from the map produced by Berra et al. (2012). The glacier coverage maps of the site are obtained from Knoflach et al. (2021).

Author contributions. All authors participated in the conceptualization, methodology, data acquisition, design of the experiment, and discussion on the results. XF carried out the formal analyses and investigations. The hydrological *WaSiM* model is calibrated by XF and FH. XF

wrote the original manuscript and visualized all the results, all co-authors contributed to the editing and review. BS and GC supervised the work and acquired the project funding.

Competing interests. The authors declare that there is no competing interest in this work.

Acknowledgements. We acknowledge the valuable discussions about the hydrological modeling results with the *WaSiM* developer Jörg Schulla. We thank the technician Mr. Michael Tarantik and the students at the Technical University of Munich for measuring and obtaining the hydrological data in the Martell Valley. We thank Dr. Natalie Ceperley at University of Bern for the laboratory analysis of the stable water isotopes. We thank the project partners in Eurac Italy for providing the information on the catchment land cover, geology, and soil properties, also thank the official authorities of Autonomous Province of Bolzano in South Tyrol, Institute of Atmospheric and Cryospheric Sciences of the University of Innsbruck, Meteo Trentino in Italy for providing the research data. XF, FH, and GC acknowledge the support of the German Research Foundation (DFG) research unit (FOR2793/2) investigating the "Sensitivity of High Alpine Geosystems to Climate Change since 1850" (SEHAG) under grant CH981/3-2. XF and BS acknowledge the Swiss National Science Foundation (SNSF) grant (200020E-204030) for "SEHAG Subproject 2 -Impact of climate change on groundwater storage in high Alpine catchments: from observation to model predictions".

References

Abhervé, R., Roques, C., Gauvain, A., Longuevergne, L., Louaisil, S., Aquilina, L., and de Dreuzy, J.-R.: Calibration of groundwater seepage against the spatial distribution of the stream network to assess catchment-scale hydraulic properties, Hydrology and Earth System Sciences, 27, 3221–3239, https://doi.org/10.5194/hess-27-3221-2023, 2023.

Ala-aho, P., Soulsby, C., Wang, H., and Tetzlaff, D.: Integrated surface-subsurface model to investigate the role of groundwater in headwater catchment runoff generation: A minimalist approach to parameterisation, Journal of Hydrology, 547, 664–677, https://doi.org/10.1016/j.jhydrol.2017.02.023, 2017.

Altmann, M., Fischer, P., Haas, F., Pfeiffer, M., Ramskogler, K., Rom, J., Kara-Timmermann, D., Himmelstoß, T., Heckmann, T., and Becht, M.: Simulation of soil erosion in the Little Ice Age glacier foreland of the Zufallferner (South Tyrol, Italy) using Erosion-3D, EGU General Assembly Conference Abstracts, pp. EGU25–5734, https://doi.org/10.5194/egusphere-egu25-5734, 2025.

Appels, W. M., Bogaart, P. W., and van der Zee, S. E.: Feedbacks between shallow groundwater dynamics and surface topography on runoff generation in flat fields, Water Resources Research, 53, 10 336–10 353, https://doi.org/10.1002/2017WR020727, 2017.

Aquanty, I.: HydroGeoSphere user manual, https://hydrogeosphere.blob.core.windows.net/hydrogeosphere/hgs/hydrosphere_ref.pdf, 2016.

Arnoux, M., Brunner, P., Schaefli, B., Mott, R., Cochand, F., and Hunkeler, D.: Low-flow behavior of alpine catchments with varying quaternary cover under current and future climatic conditions, Journal of hydrology, 592, 125 591, https://doi.org/10.1016/j.jhydrol.2020.125591, 2021.

Aubry-Wake, C., McNamara, G., Somers, L. D., McKenzie, J. M., Pomeroy, J. W., and Hellström, R.: Sensitivity of surface water and groundwater contributions to streamflow in a tropical glacierized basin under climate change scenarios, Environmental Research Letters, 19, 114 036, https://doi.org/10.1088/1748-9326/ad7c68, 2024.

Autonome Province of Bolzano: Vedretta Lunga Langenferner, Glacier report, 142, 2007.

Avanzi, F., Munerol, F., Milelli, M., Gabellani, S., Massari, C., Girotto, M., Cremonese, E., Galvagno, M., Bruno, G., Morra di Cella, U., et al.: Winter snow deficit was a harbinger of summer 2022 socio-hydrologic drought in the Po Basin, Italy, Communications Earth & Environment, 5, 64, https://doi.org/10.1038/s43247-024-01222-z, 2024.

Bahr, D. B., Meier, M. F., and Peckham, S. D.: The physical basis of glacier volume-area scaling, Journal of Geophysical Research: Solid Earth, 102, 20 355–20 362, https://doi.org/10.1029/97JB01696, 1997.

Bahr, D. B., Pfeffer, W. T., and Kaser, G.: A review of volume-area scaling of glaciers, Reviews of Geophysics, 53, 95–140, https://doi.org/10.1002/2014RG000470, 2015.

Banerjee, A., Kang, S., Guo, W., Meadows, M. E., Wang, W., Sengupta, D., and Zhang, T.: Glacier retreat and lake outburst floods in the central Himalayan region from 2000 to 2022, Natural Hazards, 120, 5485–5508, https://doi.org/10.1007/s11069-024-06415-5, 2024.

Batjes, N. H., Ribeiro, E., and Van Oostrum, A.: Standardised soil profile data to support global mapping and modelling (WoSIS snapshot 2019), Earth System Science Data, 12, 299–320, https://doi.org/10.5194/essd-12-299-2020, 2020.

Berra, F., Sciesa, E., Mazoccola, D., Mair, V., Longhin, M., Gazzola, D., and Guglielmin, M.: Kartiergebiete des Grundgebirges und der Permo-Mesozoischen Sedimentabfolge im Masstab 1:10000, 2012.

Beven, K. J. and Kirkby, M. J.: A physically based, variable contributing area model of basin hydrology, Hydrological Sciences Journal, 24, 43–69, https://doi.org/10.1080/02626667909491834, 1979.

Bonotto, G., Peterson, T. J., Fowler, K., and Western, A. W.: Identifying causal interactions between groundwater and streamflow using convergent cross-mapping, Water Resources Research, 58, e2021WR030 231, https://doi.org/10.1029/2021WR030231, 2022.

Borzi, I.: Modeling groundwater resources in data-scarce regions for sustainable management: Methodologies and limits, Hydrology, 12, 11, https://doi.org/10.3390/hydrology12010011, 2025.

Bosco, C., de Rigo, D., Dewitte, O., Poesen, J., and Panagos, P.: Modelling soil erosion at European scale: towards harmonization and reproducibility, Natural Hazards and Earth System Sciences, 15, 225–245, https://doi.org/10.5194/nhess-15-225-2015, 2015.

Brighenti, S., Engel, M., Dinale, R., Tirler, W., Voto, G., and Comiti, F.: Isotopic and chemical signatures of high mountain rivers in catchments with contrasting glacier and rock glacier cover, Journal of Hydrology, 623, 129 779, https://doi.org/10.1016/j.jhydrol.2023.129779, 2023.

Bronstert, A., Niehoff, D., and Schiffler, G. R.: Modelling infiltration and infiltration excess: The importance of fast and local processes, Hydrological Processes, 37, e14 875, https://doi.org/10.1002/hyp.14875, 2023.

Brutsaert, W.: Evaporation into the atmosphere, Kluwer Academic Publishers, Dordrecht, 1982.

Carletti, F., Michel, A., Casale, F., Burri, A., Bocchiola, D., Bavay, M., and Lehning, M.: A comparison of hydrological models with different level of complexity in Alpine regions in the context of climate change, Hydrology and Earth System Sciences, 26, 3447–3475, https://doi.org/10.5194/hess-26-3447-2022, 2022.

Ceperley, N., Zuecco, G., Beria, H., Carturan, L., Michelon, A., Penna, D., Larsen, J., and Schaefli, B.: Seasonal snow cover decreases young water fractions in high Alpine catchments, Hydrological Processes, 34, 4794–4813, https://doi.org/10.1002/hyp.13937, 2020.

Chen, J. and Ohmura, A.: Estimation of Alpine glacier water resources and their change since the 1870s, IAHS publication, 193, 127–135, 1990.

Chen, Z., Lucianetti, G., and Hartmann, A.: Understanding groundwater storage and drainage dynamics of a high mountain catchment with complex geology using a semi-distributed process-based modelling approach, Journal of Hydrology, 625, 130 067, https://doi.org/10.1016/j.jhydrol.2023.130067, 2023.

Coderre, P., Knoben, W., Thébault, C., Vásquez, N., Clark, M., and Pietroniro, A.: The impact of benchmark selection on spatial patterns of model evaluation metrics, EGU General Assembly, https://doi.org/10.5194/egusphere-egu26-15343, 2026.

Collaud Coen, M. and Vogt, F. P.: mannkendall/Matlab: Bug fix: prob_mk_n (v1.1.0)., https://doi.org/10.5281/zenodo.4495589, 2021.

Collaud Coen, M., Andrews, E., Bigi, A., Martucci, G., Romanens, G., Vogt, F. P., and Vuilleumier, L.: Effects of the prewhitening method, the time granularity, and the time segmentation on the Mann–Kendall trend detection and the associated Sen's slope, Atmospheric measurement techniques, 13, 6945–6964, https://doi.org/10.5194/amt-13-6945-2020, 2020.

CORINE Land Cover: CORINE Land Cover Data 2018, https://land.copernicus.eu/en/products/corine-land-cover, 2018.

Cornelissen, T., Diekkrüger, B., and Giertz, S.: A comparison of hydrological models for assessing the impact of land use and climate change on discharge in a tropical catchment, Journal of Hydrology, 498, 221–236, https://doi.org/10.1016/j.jhydrol.2013.06.016, 2013.

Coxon, G., Freer, J., Lane, R., Dunne, T., Knoben, W. J., Howden, N. J., Quinn, N., Wagener, T., and Woods, R.: DECIPHeR v1: dynamic fluxEs and connectivity for predictions of HydRology, Geoscientific Model Development, 12, 2285–2306, https://doi.org/10.5194/gmd-12-2285-2019, 2019.

Di Baldassarre, G. and Montanari, A.: Uncertainty in river discharge observations: a quantitative analysis, Hydrology and Earth System Sciences, 13, 913–921, https://doi.org/10.5194/hess-13-913-2009, 2009.

di Bolzano Alto Adige, P. A.: Digitales Geländemodell (DGM 2,5m), https://data.civis.bz.it/de/dataset/modello-digitale-del-terreno-dtm-25m, 2006.

Dobler, C. and Pappenberger, F.: Global sensitivity analyses for a complex hydrological model applied in an Alpine watershed, Hydrological Processes, 27, 3922–3940, https://doi.org/10.1002/hyp.9520, 2013.

Dong, C.: Remote sensing, hydrological modeling and in situ observations in snow cover research: A review, Journal of Hydrology, 561, 573–583, https://doi.org/10.1016/j.jhydrol.2018.04.027, 2018.

Drenkhan, F., Buytaert, W., Mackay, J. D., Barrand, N. E., Hannah, D. M., and Huggel, C.: Looking beyond glaciers to understand mountain water security, Nature Sustainability, 6, 130–138, https://doi.org/10.1038/s41893-022-00996-4, 2023.

Duncan, C., Masek, J., and Fielding, E.: How steep are the Himalaya? Characteristics and implications of along-strike topographic variations, Geology, 31, 75–78, https://doi.org/10.1130/0091-7613(2003)031<0075:HSATHC>2.0.CO;2, 2003.

Dunne, T.: Relation of field studies and modeling in the prediction of storm runoff, Journal of hydrology, 65, 25–48, https://doi.org/10.1016/0022-1694(83)90209-3, 1983.

Dussaillant, I., Hugonnet, R., Huss, M., Berthier, E., Bannwart, J., Paul, F., and Zemp, M.: Annual mass change of the world's glaciers from 1976 to 2024 by temporal downscaling of satellite data with in situ observations, Earth System Science Data, 17, 1977–2006, https://doi.org/10.5194/essd-17-1977-2025, 2025.

Ebbing, J., England, R., Korja, T., Lauritsen, T., Olesen, O., Stratford, W., and Weidle, C.: Structure of the Scandes lithosphere from surface to depth, Tectonophysics, 536, 1–24, https://doi.org/10.1016/j.tecto.2012.02.016, 2012.

Engdahl, N. B.: Impacts of permeability uncertainty in a coupled surface-subsurface flow model under perturbed recharge scenarios, Water Resources Research, 60, e2023WR035 975, https://doi.org/10.1029/2023WR035975, 2024.

Fan, X., Goeppert, N., and Goldscheider, N.: Quantifying the historic and future response of karst spring discharge to climate variability and change at a snow-influenced temperate catchment in central Europe, Hydrogeology Journal, 31, 2213–2229, https://doi.org/10.1007/s10040-023-02703-9, 2023a.

Fan, X., Peterson, T. J., Henley, B. J., and Arora, M.: Groundwater sensitivity to climate variations across Australia, Water Resources Research, 59, e2023WR035 036, https://doi.org/10.1029/2023WR035036, 2023b.

Fan, X., Schaefli, B., Hofmeister, F., and Chiogna, G.: When the Past Matters: How Model Initialization Can Lead to Surprises in Long-Term Simulations in Glaciated Environments, Hydrological Processes, 40, e70 507, https://doi.org/10.1002/hyp.70507, 2026.

FAO & IIASA: Harmonized World Soil Database Version 2.0. Rome and Laxenburg., https://data.isric.org/geonetwork/srv/eng/catalog.search#/metadata/54aebf11-ec73-4ff8-bf6c-ecff4b0725ea, 2023.

Fatichi, S., Rimkus, S., Burlando, P., Bordoy, R., and Molnar, P.: High-resolution distributed analysis of climate and anthropogenic changes on the hydrology of an Alpine catchment, Journal of Hydrology, 525, 362–382, https://doi.org/10.1016/j.jhydrol.2015.03.036, 2015.

Fatichi, S., Vivoni, E. R., Ogden, F. L., Ivanov, V. Y., Mirus, B., Gochis, D., Downer, C. W., Camporese, M., Davison, J. H., Ebel, B., et al.: An overview of current applications, challenges, and future trends in distributed process-based models in hydrology, Journal of Hydrology, 537, 45–60, https://doi.org/10.1016/j.jhydrol.2016.03.026, 2016.

Förster, K., Garvelmann, J., Meißl, G., and Strasser, U.: Modelling forest snow processes with a new version of WaSiM, Hydrological Sciences Journal, 63, 1540–1557, 2018.

Freudiger, D., Kohn, I., Seibert, J., Stahl, K., and Weiler, M.: Snow redistribution for the hydrological modeling of alpine catchments, Wiley Interdisciplinary Reviews: Water, 4, e1232, https://doi.org/10.1002/wat2.1232, 2017.

Galos, S. P., Klug, C., Maussion, F., Covi, F., Nicholson, L., Rieg, L., Gurgiser, W., Mölg, T., and Kaser, G.: Reanalysis of a 10-year record (2004–2013) of seasonal mass balances at Langenferner/Vedretta Lunga, Ortler Alps, Italy, The Cryosphere, 11, 1417–1439, https://doi.org/10.5194/tc-11-1417-2017, 2017.

Garambois, P.-A., Roux, H., Larnier, K., Castaings, W., and Dartus, D.: Characterization of process-oriented hydrologic model behavior with temporal sensitivity analysis for flash floods in Mediterranean catchments, Hydrology and Earth System Sciences, 17, 2305–2322, https://doi.org/10.5194/hess-17-2305-2013, 2013.

Gauthier, T. D.: Detecting trends using Spearman's rank correlation coefficient, Environmental Forensics, 2, 359–362, https://doi.org/10.1006/enfo.2001.0061, 2001.

Glaser, B., Antonelli, M., Chini, M., Pfister, L., and Klaus, J.: Mapping surface-saturation dynamics with thermal infrared imagery, Hydrology and Earth System Sciences, 22, 5987–6003, https://doi.org/10.5194/hess-22-5987-2018, 2018.

Gruber, S.: A mass-conserving fast algorithm to parameterize gravitational transport and deposition using digital elevation models, Water Resources Research, 43, 2007.

Guyennon, N., Valt, M., Salerno, F., Petrangeli, A. B., and Romano, E.: Estimating the snow water equivalent from snow depth measurements in the Italian Alps, Cold Regions Science and Technology, 167, 102 859, https://doi.org/10.1016/j.coldregions.2019.102859, 2019.

Hayashi, M.: Alpine hydrogeology: The critical role of groundwater in sourcing the headwaters of the world, Groundwater, 58, 498–510, https://doi.org/10.1111/gwat.12965, 2019.

Hock, R.: Modelling of glacier melt and discharge, Ph.D. thesis, ETH Zurich, 1998.

Hock, R.: A distributed temperature-index ice-and snowmelt model including potential direct solar radiation, Journal of Glaciology, 45, 101–111, https://doi.org/10.3189/S0022143000003087, 1999.

Hofmeister, F., Arias-Rodriguez, L. F., Premier, V., Marin, C., Notarnicola, C., Disse, M., and Chiogna, G.: Intercomparison of Sentinel-2 and modelled snow cover maps in a high-elevation Alpine catchment, Journal of Hydrology X, 15, 100 123, https://doi.org/10.1016/j.hydroa.2022.100123, 2022.

Hofmeister, F., Graziano, F., Marcolini, G., Willems, W., Disse, M., and Chiogna, G.: Quality assessment of hydrometeorological observational data and their influence on hydrological model results in Alpine catchments, Hydrological Sciences Journal, 68, 552–571, https://doi.org/10.1080/02626667.2023.2172335, 2023a.

Hofmeister, F., Venegas, B. R., Sentlinger, G., Tarantik, M., Blume, T., Disse, M., and Chiogna, G.: Automated streamflow measurements in high-elevation Alpine catchments, River Research and Applications, 39, 2079–2091, https://doi.org/10.1002/rra.4203, 2023b.

Höge, M., Kauzlaric, M., Siber, R., Schönenberger, U., Horton, P., Schwanbeck, J., Floriancic, M. G., Viviroli, D., Wilhelm, S., Sikorska-Senoner, A. E., et al.: CAMELS-CH: hydro-meteorological time series and landscape attributes for 331 catchments in hydrologic Switzerland, Earth System Science Data, 15, 5755–5784, https://doi.org/10.5194/essd-15-5755-2023, 2023.

Horton, P., Schaefli, B., and Kauzlaric, M.: Why do we have so many different hydrological models? A review based on the case of Switzerland, Wiley Interdisciplinary Reviews: Water, 9, e1574, https://doi.org/10.1002/wat2.1574, 2022.

IPCC: Climate change 2021: The physical science basis. Contribution of working group I to the sixth assessment report of the intergovernmental panel on climate change, Cambridge University Press, 2021.

Isotta, F. A., Frei, C., and Schwanbeck, J.: Mean Precipitation throughout the Alps 1971–2008, in: Data and Analysis Platform, Hydrological Atlas of Switzerland, https://hydromaps.ch/#en/7/46.111/10.898/bl_hds--b02_b0200_alpine_precip_y_1971_2008v1_0$0/NULL, 2018.

Jansson, P. and Karlberg, L.: Coupled heat and mass transfer model for soil-plant-atmosphere systems, Royal Institute of Technology, Dept of Civil and Environmental Engineering, Stockholm, 2011.

Jarvis, A., Reuter, H., Nelson, A., and Guevara, E.: Hole-filled seamless SRTM data V4, http://srtm.csi.cgiar.org, 2008.

Kendall, M.: Rank correlation methods, Charles Griffin, London, 196 pp, 1955.

Knoflach, B., Ramskogler, K., Talluto, M., Hofmeister, F., Haas, F., Heckmann, T., Pfeiffer, M., Piermattei, L., Ressl, C., Wimmer, M. H., et al.: Modelling of vegetation dynamics from satellite time series to determine proglacial primary succession in the course of global warming—A case study in the upper Martell Valley (Eastern Italian Alps), Remote Sensing, 13, 4450, https://doi.org/10.3390/rs13214450, 2021.

Krause, S., Bronstert, A., and Zehe, E.: Groundwater–surface water interactions in a North German lowland floodplain–implications for the river discharge dynamics and riparian water balance, Journal of Hydrology, 347, 404–417, https://doi.org/10.1016/j.jhydrol.2007.09.028, 2007.

Kumar, R., Samaniego, L., and Attinger, S.: Implications of distributed hydrologic model parameterization on water fluxes at multiple scales and locations, Water Resources Research, 49, 360–379, https://doi.org/10.1029/2012WR012195, 2013.

Liu, J., Liu, J., Liu, M., Tian, S., Liu, Y., Yang, W., and Liu, Y.: Development of an alpine hydrological model considering the recharge of stream water to alluvial plain aquifers, Environmental Modelling and Software, p. 106567, https://doi.org/10.1016/j.envsoft.2025.106567, 2025.

Liu, M., Pei, H., and Shen, Y.: Evaluating dynamics of GRACE groundwater and its drought potential in Taihang Mountain Region, China, Journal of Hydrology, 612, 128 156, https://doi.org/10.1016/j.jhydrol.2022.128156, 2022.

Livneh, B., Kumar, R., and Samaniego, L.: Influence of soil textural properties on hydrologic fluxes in the Mississippi river basin, Hydrological Processes, 29, 4638–4655, https://doi.org/10.1002/hyp.10601, 2015.

Mann, H.: Nonparametric tests against trend, Econometrica, 13, 245–259, https://doi.org/10.2307/1907187, 1945.

Marcolini, G., Bellin, A., Disse, M., and Chiogna, G.: Variability in snow depth time series in the Adige catchment, Journal of Hydrology: Regional Studies, 13, 240–254, https://doi.org/10.1016/j.ejrh.2017.08.007, 2017.

Matiu, M., Jacob, A., and Notarnicola, C.: Daily MODIS snow cover maps for the European Alps from 2002 onwards at 250 m horizontal resolution along with a nearly cloud-free version, Data, 5, 1, https://doi.org/10.3390/data5010001, 2019.

Matiu, M., Crespi, A., Bertoldi, G., Carmagnola, C. M., Marty, C., Morin, S., Schöner, W., Cat Berro, D., Chiogna, G., De Gregorio, L., et al.: Observed snow depth trends in the European Alps: 1971 to 2019, The Cryosphere, 15, 1343–1382, https://doi.org/10.5194/tc-15-1343-2021, 2021.

Mazzilli, N., Guinot, V., Jourde, H., Lecoq, N., Labat, D., Arfib, B., Baudement, C., Danquigny, C., Dal Soglio, L., and Bertin, D.: KarstMod: A modelling platform for rainfall-discharge analysis and modelling dedicated to karst systems, Environmental Modelling & Software, 122, 103 927, https://doi.org/10.1016/j.envsoft.2017.03.015, 2019.

McGuire, K. J., Klaus, J., and Jackson, C. R.: JAMES BUTTLE REVIEW: Interflow, subsurface stormflow and throughflow: A synthesis of field work and modelling, Hydrological Processes, 38, e15 263, https://doi.org/10.1002/hyp.15263, 2024.

Meier, A.: Hydrological insights into glacier melt discharge: A multi-method approach using isotopes in a small alpine environment above 1745 m.a.s.l., Master's thesis, University of Bern, https://www.geography.unibe.ch/unibe/portal/fak_naturwis/e_geowiss/c_igeogr/content/e39592/e1608235/e1608239/pane1608241/e1611621/Meier.Anna_2024_komprimiert_ger.pdf, 2024.

Michel, A., Schaefli, B., Wever, N., Zekollari, H., Lehning, M., and Huwald, H.: Future water temperature of rivers in Switzerland under climate change investigated with physics-based models, Hydrology and Earth System Sciences, 26, 1063–1087, https://doi.org/10.5194/hess-26-1063-2022, 2022.

Monteith, J.: Evaporation and surface temperature, Quarterly Journal of the Royal Meteorological Society, 107, 1–27, 1981.

Müller, T., Lane, S. N., and Schaefli, B.: Towards a hydrogeomorphological understanding of proglacial catchments: an assessment of groundwater storage and release in an Alpine catchment, Hydrology and Earth System Sciences, 26, 6029–6054, https://doi.org/10.5194/hess-26-6029-2022, 2022.

Müller, T., Roncoroni, M., Mancini, D., Lane, S. N., and Schaefli, B.: Current and future roles of meltwater–groundwater dynamics in a proglacial Alpine outwash plain, Hydrology and Earth System Sciences, 28, 735–759, https://doi.org/10.5194/hess-28-735-2024, 2024.

Nan, Y., Tian, L., He, Z., Tian, F., and Shao, L.: The value of water isotope data on improving process understanding in a glacierized catchment on the Tibetan Plateau, Hydrology and Earth System Sciences Discussions, 2021, 1–40, https://doi.org/10.5194/hess-25-3653-2021, 2021.

Nan, Y., Tian, F., McDonnell, J., Ni, G., Tian, L., Li, Z., Yan, D., Xia, X., Wang, T., Han, S., et al.: Glacier meltwater has limited contributions to the total runoff in the major rivers draining the Tibetan Plateau, npj Climate and Atmospheric Science, 8, 155, https://doi.org/10.1038/s41612-025-01060-6, 2025.

Nash, J. E. and Sutcliffe, J. V.: River flow forecasting through conceptual models part I — a discussion of principles, Journal of Hydrology, 10, 282–290, 1970.

Owen, L. A. and Dortch, J. M.: Nature and timing of Quaternary glaciation in the Himalayan–Tibetan orogen, Quaternary Science Reviews, 88, 14–54, https://doi.org/10.1016/j.quascirev.2013.11.016, 2014.

Paillex, A., Siebers, A. R., Ebi, C., Mesman, J., and Robinson, C. T.: High stream intermittency in an alpine fluvial network: Val Roseg, Switzerland, Limnology and Oceanography, 65, 557–568, https://doi.org/10.1002/lno.11324, 2020.

Paniconi, C. and Putti, M.: Physically based modeling in catchment hydrology at 50: Survey and outlook, Water Resources Research, 51, 7090–7129, https://doi.org/10.1002/2015WR017780, 2015.

Paschalis, A., Bonetti, S., Guo, Y., and Fatichi, S.: On the uncertainty induced by pedotransfer functions in terrestrial biosphere modeling, Water Resources Research, 58, e2021WR031 871, https://doi.org/10.1029/2021WR031871, 2022.

Pistocchi, A.: Simple estimation of snow density in an Alpine region, Journal of Hydrology: Regional Studies, 6, 82–89, https://doi.org/10.1016/j.ejrh.2016.03.004, 2016.

Pomeroy, J., Gray, D., Brown, T., Hedstrom, N., Quinton, W., Granger, R., and Carey, S.: The cold regions hydrological model: a platform for basing process representation and model structure on physical evidence, Hydrological Processes, 21, 2650–2667, https://doi.org/10.1002/hyp.6787, 2007.

Pourali, S., Arrowsmith, C., Chrisman, N., Matkan, A., and Mitchell, D.: Topography wetness index application in flood-risk-based land use planning, Applied Spatial Analysis and Policy, 9, 39–54, https://doi.org/10.1007/s12061-014-9130-2, 2016.

Puspitarini, H. D., François, B., Zaramella, M., Brown, C., and Borga, M.: The impact of glacier shrinkage on energy production from hydropower-solar complementarity in alpine river basins, Science of The Total Environment, 719, 137 488, https://doi.org/10.1016/j.scitotenv.2020.137488, 2020.

Ramskogler, K., Knoflach, B., Elsner, B., Erschbamer, B., Haas, F., Heckmann, T., Hofmeister, F., Piermattei, L., Ressl, C., Trautmann, S., et al.: Primary succession and its driving variables–a sphere-spanning approach applied in proglacial areas in the upper Martell Valley (Eastern Italian Alps), Biogeosciences, 20, 2919–2939, https://doi.org/10.5194/bg-20-2919-2023, 2023.

Reato, A., Borzi, G., Martínez, O. A., and Carol, E.: Role of rock glaciers and other high-altitude depositional units in the hydrology of the mountain watersheds of the Northern Patagonian Andes, Science of the Total Environment, 824, 153 968, https://doi.org/10.1016/j.scitotenv.2022.153968, 2022.

Rehfeldt, K. R., Boggs, J. M., and Gelhar, L. W.: Field study of dispersion in a heterogeneous aquifer: 3. Geostatistical analysis of hydraulic conductivity, Water resources research, 28, 3309–3324, https://doi.org/10.1029/92WR01758, 1992.

Richards, L. A.: Capillary conduction of liquids through porous mediums, Physics, 1, 318–333, https://doi.org/10.1063/1.1745010, 1931.

Rounce, D. R., Hock, R., Maussion, F., Hugonnet, R., Kochtitzky, W., Huss, M., Berthier, E., Brinkerhoff, D., Compagno, L., Copland, L., et al.: Global glacier change in the 21st century: Every increase in temperature matters, Science, 379, 78–83, https://doi.org/10.1126/science.abo1324, 2023.

Ruelland, D.: Potential of snow data to improve the consistency and robustness of a semi-distributed hydrological model using the SAFRAN input dataset, Journal of Hydrology, 631, 130 820, https://doi.org/10.1016/j.jhydrol.2024.130820, 2024.

Schaefli, B. and Huss, M.: Integrating point glacier mass balance observations into hydrologic model identification, Hydrology and Earth System Sciences, 15, 1227–1241, https://doi.org/10.5194/hess-15-1227-2011, 2011.

Schaefli, B., Hingray, B., Niggli, M., and Musy, A.: A conceptual glacio-hydrological model for high mountainous catchments, Hydrology and Earth System Sciences, 9, 95–109, 2005.

Schaefli, B., Nicótina, L., Imfeld, C., Da Ronco, P., Bertuzzo, E., and Rinaldo, A.: SEHR-ECHO v1.0: a Spatially Explicit Hydrologic Response model for ecohydrologic applications, Geoscientific Model Development, 7, 2733–2746, https://doi.org/10.5194/gmd-7-2733-2014, 2014.

Schaefli, B., Manso, P., Fischer, M., Huss, M., and Farinotti, D.: The role of glacier retreat for Swiss hydropower production, Renewable Energy, 132, 615–627, https://doi.org/10.1016/j.renene.2018.07.104, 2019.

Schaffhauser, T., Tuo, Y., Hofmeister, F., Chiogna, G., Huang, J., Merk, F., and Disse, M.: SWAT-GL: A new glacier routine for the hydrological model SWAT, JAWRA Journal of the American Water Resources Association, 60, 755–766, https://doi.org/10.1111/1752-1688.13199, 2024.

Schlögl, S., Marty, C., Bavay, M., and Lehning, M.: Sensitivity of Alpine3D modeled snow cover to modifications in DEM resolution, station coverage and meteorological input quantities, Environmental Modelling & Software, 83, 387–396, https://doi.org/10.1016/j.envsoft.2016.02.017, 2016.

Schmid, E.: High alpine winter discharge development in Switzerland, https://doi.org/10.5281/zenodo.13685009, 2024.

Schulla, J.: Flussgebietsmodellierung und Wasserhaushalts-Simulation mit WaSiM-Modellbeschreibung. Eidgenössische technische Hochschule Zürich, Zürich, 189pp, 1997.

Schulla, J.: Model Description WaSiM (Water balance Simulation Model), http://www.wasim.ch/downloads/doku/wasim/wasim_2024_en.pdf, 2024.

Seibert, J. and Bergström, S.: A retrospective on hydrological catchment modelling based on half a century with the HBV model, Hydrology and Earth System Sciences, 26, 1371–1388, https://doi.org/10.5194/hess-26-1371-2022, 2022.

Sen, P.: Estimates of the regression coefficient based on Kendall's tau, Journal of the American Statistical Association, 63, 1379–1389, https://doi.org/10.1080/01621459.1968.10480934, 1968.

Shrestha, M., Wang, L., Koike, T., Tsutsui, H., Xue, Y., and Hirabayashi, Y.: Correcting basin-scale snowfall in a mountainous basin using a distributed snowmelt model and remote-sensing data, Hydrology and Earth System Sciences, 18, 747–761, https://doi.org/10.5194/hess-18-747-2014, 2014.

Sivelle, V., Cinkus, G., Mazzilli, N., Labat, D., Arfib, B., Massei, N., Cousquer, Y., Bertin, D., and Jourde, H.: Improvement of the Karst-Mod modelling platform for a better assessment of karst groundwater resources, Hydrology and Earth System Sciences, 29, 1259–1276, https://doi.org/10.5194/hess-29-1259-2025, 2025.

Somers, L. D. and McKenzie, J. M.: A review of groundwater in high mountain environments, Wiley Interdisciplinary Reviews: Water, 7, e1475, https://doi.org/10.1002/wat2.1475, 2020.

Somers, L. D., Gordon, R. P., McKenzie, J. M., Lautz, L. K., Wigmore, O., Glose, A., Glas, R., Aubry-Wake, C., Mark, B., Baraer, M., et al.: Quantifying groundwater–surface water interactions in a proglacial valley, Cordillera Blanca, Peru, Hydrological Processes, 30, 2915–2929, https://doi.org/10.1002/hyp.10912, 2016.

Stutenbecker, L., Costa, A., and Schlunegger, F.: Lithological control on the landscape form of the upper Rhône Basin, Central Swiss Alps, Earth Surface Dynamics, 4, 253–272, https://doi.org/10.5194/esurf-4-253-2016, 2016.

Talbot, F., Sylvain, J.-D., Drolet, G., Poulin, A., and Arsenault, R.: Enhancing physically based and distributed hydrological model calibration through internal state variable constraints, EGUsphere, 2024, 1–42, https://doi.org/10.5194/egusphere-2024-3353, 2024.

Thornton, J. M., Brauchli, T., Mariethoz, G., and Brunner, P.: Efficient multi-objective calibration and uncertainty analysis of distributed snow simulations in rugged alpine terrain, Journal of Hydrology, 598, 126 241, https://doi.org/10.1016/j.jhydrol.2021.126241, 2021.

Thornton, J. M., Therrien, R., Mariéthoz, G., Linde, N., and Brunner, P.: Simulating fully-integrated hydrological dynamics in complex alpine headwaters: potential and challenges, Water Resources Research, 58, e2020WR029 390, https://doi.org/10.1029/2020WR029390, 2022.

Trancoso, R., Larsen, J. R., McAlpine, C., McVicar, T. R., and Phinn, S.: Linking the Budyko framework and the Dunne diagram, Journal of Hydrology, 535, 581–597, https://doi.org/10.1016/j.jhydrol.2016.02.017, 2016.

Trinh, T., Kavvas, M., Ishida, K., Ercan, A., Chen, Z., Anderson, M., Ho, C., and Nguyen, T.: Integrating global land-cover and soil datasets to update saturated hydraulic conductivity parameterization in hydrologic modeling, Science of the Total Environment, 631, 279–288, https://doi.org/10.1016/j.scitotenv.2018.02.267, 2018.

Tuo, Y., Marcolini, G., Disse, M., and Chiogna, G.: A multi-objective approach to improve SWAT model calibration in alpine catchments, Journal of Hydrology, 559, 347–360, https://doi.org/10.1016/j.jhydrol.2018.02.055, 2018.

van Tiel, M., Aubry-Wake, C., Somers, L., Andermann, C., Avanzi, F., Baraer, M., Chiogna, G., Daigre, C., Das, S., Drenkhan, F., et al.: Cryosphere–groundwater connectivity is a missing link in the mountain water cycle, Nature Water, pp. 1–14, https://doi.org/10.1038/s44221-024-00277-8, 2024.

Vereecken, H., Huisman, J., Bogena, H., Vanderborght, J., Vrugt, J., and Hopmans, J.: On the value of soil moisture measurements in vadose zone hydrology: A review, Water resources research, 44, https://doi.org/10.1029/2008WR006829, 2008.

Voigt, C., Schulz, K., Koch, F., Wetzel, K.-F., Timmen, L., Rehm, T., Pflug, H., Stolarczuk, N., Förste, C., and Flechtner, F.: Introduction of a superconducting gravimeter as novel hydrological sensor for the Alpine research catchment Zugspitze, Hydrology and Earth System Sciences, 25, 5047–5064, https://doi.org/10.5194/hess-25-5047-2021, 2021.

Wang, S., Yuan, R., Tang, C., Song, X., Currell, M., Yang, Z., and Sheng, Z.: Combination of CFCs and stable isotopes to characterize the mechanism of groundwater–surface water interactions in a headwater basin of the North China Plain, Hydrological Processes, 32, 1571–1587, https://doi.org/10.1002/hyp.11494, 2018.

Warscher, M., Strasser, U., Kraller, G., Marke, T., Franz, H., and Kunstmann, H.: Performance of complex snow cover descriptions in a distributed hydrological model system: A case study for the high Alpine terrain of the Berchtesgaden Alps, Water Resources Research, 49, 2619–2637, https://doi.org/10.1002/wrcr.20219, 20, 2013.

Wechsler, T., Stähli, M., Jorde, K., Zappa, M., and Schaefli, B.: The future of Alpine Run-of-River hydropower production: Climate change, environmental flow requirements, and technical production potential, Science of the Total Environment, 890, 163 934, https://doi.org/10.1016/j.scitotenv.2023.163934, 2023.

Welch, R. M. and Shaw, J. H.: Structural styles and kinematic evolution of the Front Ranges of the Southern Canadian Rockies, Geosphere, 21, 605–636, https://doi.org/10.1130/GES02814.1, 2025.

Winkler, M., Schellander, H., and Gruber, S.: Snow water equivalents exclusively from snow depths and their temporal changes: the Δsnow model, Hydrology and Earth System Sciences, 25, 1165–1187, https://doi.org/10.5194/hess-25-1165-2021, 2021.

Woodbury, A. D. and Sudicky, E. A.: The geostatistical characteristics of the Borden aquifer, Water Resources Research, 27, 533–546, https://doi.org/10.1029/90WR02545, 1991.

Xiang, L., Wang, H., Steffen, H., Wu, P., Jia, L., Jiang, L., and Shen, Q.: Groundwater storage changes in the Tibetan Plateau and adjacent areas revealed from GRACE satellite gravity data, Earth and Planetary Science Letters, 449, 228–239, https://doi.org/10.1016/j.epsl.2016.06.002, 2016.

Xie, S., Zeng, C., Zhang, F., Wang, G., and Xiao, X.: Defining lateral subsurface flow and identifying its water sources in an alpine-permafrost hillslope, Catena, 236, 107 765, https://doi.org/10.1016/j.catena.2023.107765, 2024.

Zhang, Z., Gu, Z., Hu, K., Hu, K., Xu, Y., and Zhao, J.: Spatial variability between glacier mass balance and environmental factors in the High Mountain Asia, Journal of Arid Land, 14, 441–454, https://doi.org/10.1007/s40333-017-0014-z, 2022.